

submitted to The Astronomical Journal on June 27, 1998

**The black hole mass distribution in early-type galaxies:
cusps in HST photometry interpreted through adiabatic black hole growth**

Roeland P. van der Marel¹

Space Telescope Science Institute, 3700 San Martin Drive, Baltimore, MD 21218

arXiv:astro-ph/9806365v1 27 Jun 1998

¹STScI Fellow.

ABSTRACT

HST observations show that the surface brightness profiles of early-type galaxies have central cusps, $I \propto r^{-\gamma}$. Two characteristic profile types are observed: ‘core’ profiles have a break at a resolved radius and $\gamma \leq 0.3$ inside that radius; ‘power-law’ profiles have no clear break and $\gamma > 0.3$. With few exceptions, galaxies with $M_V < -22$ have core profiles, and galaxies with $M_V > -20.5$ have power-law profiles. Both profile types occur in galaxies with $-22 < M_V < -20.5$. We show here that these results are consistent with the hypothesis that: (i) all early-type galaxies have central BHs that grew adiabatically in homogeneous isothermal cores; and (ii) these ‘progenitor’ cores followed scaling relations similar to those of the fundamental plane.

The models studied here are the ones first proposed by Young. They predict $I \propto r^{-1/2}$ at asymptotically small radii, but $I \propto r^{-\gamma}$ at the radii observable with HST. The slope γ can take all observed values; it increases monotonically with $\mu = M_\bullet/M_{\text{core}}$. The scaling relations for early-type galaxies imply that the progenitor core mass scales with luminosity as $M_{\text{core}} \propto L^{1.5}$. If, as suggested by various arguments, the black hole (BH) mass M_\bullet scales roughly linearly with luminosity, $M_\bullet \propto L$, then $\mu \propto L^{-0.5}$. This yields larger cusp slopes in lower-luminosity galaxies. Models with BH masses and progenitor cores that obey established scaling relations predict (at the distance of the Virgo cluster) that galaxies with $M_V < -21.2$ have core profiles and galaxies with $M_V > -21.2$ have power-law profiles. This reproduces both the sense and the absolute magnitude of the observed transition. Intrinsic scatter in BH and galaxy properties can explain why both types of galaxies are observed around the transition magnitude. The observed bimodality in cusp slopes may be due to a bimodality in M_\bullet/L , with rapidly rotating disk galaxies having larger M_\bullet/L than slowly rotating boxy galaxies.

We apply the models to 46 galaxies with published HST photometry. Both core and power-law galaxies are well fitted. The models suggest a roughly linear correlation between BH mass and V-band galaxy luminosity, $\log M_\bullet \approx -1.83 + \log L$ in solar units (RMS scatter 0.33 dex). This agrees with the average relation for nearby galaxies with kinematically determined BH masses. Photometrically and kinematically determined BH masses agree to within ~ 0.25 dex RMS for galaxies that have both. These results provide additional support to the hypothesis that every galaxy (spheroid) has a central BH. The BH mass distribution inferred here is consistent with quasar statistics for a BH accretion efficiency of 4%.

The proposed scenario is not a unique way to interpret the observed surface brightness cusps of galaxies, but it explains observational correlations that are otherwise unexplained, and it yields BH masses that agree with those determined kinematically.

Subject headings: galaxies: elliptical and lenticular, cD — galaxies: kinematics and dynamics — galaxies: nuclei — galaxies: structure.

1. Introduction

The high spatial resolution of the Hubble Space Telescope (HST) has allowed astronomers to study the photometric structure of galactic nuclei with unprecedented detail. Most studies have focused on early-type galaxies and bulges, and many systems have now been imaged (e.g., Crane et al. 1993; Jaffe et al. 1994; Lauer et al. 1995; Forbes, Franx & Illingworth 1995; Carollo et al. 1997, hereafter C97). The main result is that at the $\sim 0.1''$ resolution limit of HST, virtually all galaxies have power-law surface brightness cusps, $I \propto r^{-\gamma}$, with $\gamma > 0$ and no observed transition to a homogeneous core. In addition, the surface brightness profiles fall in two categories: ‘cores’, which have a break at a resolved radius,² and ‘power-laws’, which have no clear break (Faber et al. 1997; hereafter F97). The former have $\gamma \leq 0.3$, while the latter have $\gamma > 0.3$. The nuclear properties correlate with luminosity: in general, galaxies with $M_V < -22$ have core profiles, galaxies with $M_V > -20.5$ have power-law profiles, and both profile types occur in galaxies with $-22 < M_V < -20.5$. It is the aim of the present paper to provide a quantitative framework for understanding these observations through models with massive black holes (BHs).

Black holes are believed to be responsible for the energetic processes in active galaxies and quasars (e.g., Peterson 1997; Fabian 1997). Many or most quiescent galaxies may have been active in the past, and may thus also contain BHs (Soltan 1982; Chokshi & Turner 1992). It has been well documented theoretically that the presence of a BH in the center of a stellar system induces a power-law cusp in the mass distribution, $\rho \propto r^{-p}$ at asymptotically small radii, with a corresponding cusp $I \propto r^{-q}$ in the projected surface density (at asymptotically small radii $q = \max[0, p - 1]$, but this need not be true at observationally accessible radii; e.g., Gebhardt et al. 1996). With globular clusters in mind, Bahcall & Wolf (1976) showed that $p = \frac{7}{4}$ for a system with a BH that has been present longer than the two-body relaxation time (this holds for equal mass stars; the results with a mass spectrum are more complicated, cf. Bahcall & Wolf 1977). In galaxies, the two-body relaxation time typically exceeds the Hubble time, even in the central regions (Rauch & Tremaine 1997). Young (1980) inferred $p = \frac{3}{2}$ for the case of adiabatic BH growth (i.e., growth slow compared to the dynamical time) in an isothermal sphere (see also Cipollina 1995). Quinlan, Hernquist & Sigurdsson (1995) showed that non-isothermal initial conditions may yield other values of p . Adiabatic BH growth in rotating models was studied by Lee & Goodman (1989) and Cipollina & Bertin (1994). Sigurdsson, Hernquist & Quinlan (1995) presented N -body calculations of BH growth, and discussed the relation between adiabatic invariance and the BH growth time. Scenarios in which BHs appear non-adiabatically have also been addressed. Stiavelli (1998) showed that galaxy formation by violent relaxation around a pre-existing BH yields $p = \frac{3}{2}$, as in the models of Young (1980). Accretion of an external BH can either weaken an existing cusp (Quinlan & Hernquist 1997) or create a new cusp (Nakano & Makino 1997), depending on the assumed initial structure of the accreting galaxy.

Observed power-law cusps need not necessarily be associated with BHs, for several reasons.

²The term ‘core’ is somewhat confusing because of its multiple meanings. Throughout this paper, the terms ‘core profile’ and ‘core galaxy’ will refer to (a galaxy with) a cuspy core, $I \propto r^{-\gamma}$ with $\gamma \leq 0.3$, and not to (a galaxy with) a homogeneous core, $I = \text{constant}$.

First, one of the simplest stellar dynamical equilibrium systems is the singular isothermal sphere, which has $\rho \propto r^{-2}$ and no BH (e.g., Binney & Tremaine 1987). Second, a power-law density cusp can easily be created in a stellar system through dissipational processes (Mihos & Hernquist 1994). Third, cusps can form naturally without BHs even in absence of dissipation; e.g., dissipationless simulations of galaxy formation produce dark halos with $\rho \propto r^{-1}$ near the center (e.g., Navarro, Frenk & White 1996). Hence, the fact that all galaxies observed with HST have surface brightness cusps does not necessarily imply that all galaxies have BHs (Kormendy & Richstone 1995).

We focus here on the simple models of adiabatic BH growth in a homogeneous isothermal core proposed by Young (1980). These models have been used to interpret HST photometry for two well-studied galaxies that also have kinematically determined BH masses, namely M87 and M32. Given that observed surface brightness cusps can be interpreted in so many ways, it is quite remarkable how successful the models have been for these two galaxies. The photometrically determined BH mass for M87 (Young et al. 1978; Lauer et al. 1992a) agrees within the errors to that determined kinematically (Harms et al. 1994; Macchetto et al. 1997), as is the case for M32 (Lauer et al. 1992b; van der Marel et al. 1998).

The success of Young’s models for individual galaxies justifies a more detailed investigation of their viability. We therefore study whether and how these models fit in with our general understanding of galactic nuclei, as characterized by four important observational findings: (i) surface brightness profiles have cusps; (ii) cusp slopes correlate with luminosity; (iii) nuclear properties of early-type galaxies obey scaling relations similar to those of the fundamental plane (Lauer 1985; Kormendy 1985; F97); and (iv) kinematically determined BH masses in nearby galaxies tend to scale roughly with galaxy luminosity (e.g., Kormendy & Richstone 1995; Ho 1998). The key questions that these findings pose are: (a) is it possible that all surface brightness cusps observed with HST, those in core profiles as well as those in and power-law profiles, are due to adiabatic BH growth in homogeneous cores?; (b) can this scenario naturally explain the observed correlation between nuclear cusp slope and luminosity?; (c) are the properties of the required homogeneous ‘progenitor’ cores plausible in view of the fundamental plane?; and (d) is the BH mass distribution thus implied by HST photometry consistent with that suggested by kinematical observations of nearby galaxies? The main result of the present paper is that all four questions can be answered affirmatively.

The paper is organized as follows. Section 2 presents a general description and discussion of the models. Section 3 combines the models with established scaling relations for early-type galaxies to obtain predictions for the nuclear photometric properties of these galaxies as function of galaxy luminosity. Section 4 presents model fits to HST photometry of 46 individual galaxies. Section 5 summarizes and discusses the conclusions of the paper. Some additional galaxies that did not pass the selection criteria of the main sample are discussed in Appendix A.

A Hubble constant $H_0 = 80 \text{ km s}^{-1} \text{ Mpc}^{-1}$ is used throughout this paper. This does not directly influence the data-model comparison, but does set the length, mass and luminosity scales in physical units. Specifically, distance, length and mass scale as H_0^{-1} , luminosity scales as H_0^{-2} , and mass-to-light ratio scales as H_0 . All quantities in this paper pertain to the photometric V -band.

2. The models

2.1. Calculations

We study adiabatic BH growth in spherical models. The adiabaticity implies, by definition, that the orbital actions (the radial action J_r and the angular momentum L) are conserved (e.g., Binney & Tremaine 1987). The dependence of the phase-space distribution function on the actions is therefore identical before and after BH growth. However, the BH growth does change the gravitational potential, so the relation between the actions and the phase-space coordinates is different in the initial and the final models. An explicit expression for the phase-space distribution function f of the final model, as function of the energy E and the angular momentum L , can be obtained with an iterative algorithm (Young 1980). Given a trial estimate for the mass density ρ , an iteration step proceeds as follows: use Poisson’s equation to calculate the gravitational potential generated by ρ , and add the contribution of the BH; calculate the actions in this potential on a grid in (E, L) space; calculate the distribution function $f(E, L)$ on the grid, using the fact that f is the same function of the actions as in the (pre-specified) initial model; calculate a new estimate for ρ by integration of $f(E, L)$ over velocity space. Iteration proceeds until the mass-density has converged. Projected model properties can be evaluated after convergence through straightforward numerical integration. This algorithm was implemented by, e.g., Quinlan et al. (1995). Gerry Quinlan kindly provided his software for use in this paper, and all models discussed here were calculated with this software.

2.2. Initial conditions

The assumption of adiabatic BH growth by itself is not very informative. In principle, any observed surface brightness profile is consistent with this assumption, for any arbitrary value of the assumed current BH mass.³ So to make progress one must assume some knowledge about the properties of the initial model.

The analysis here is restricted to models in which the initial system is a (non-singular) isothermal sphere, as in Young (1980). The model predictions at large radii will not be used, so the only relevant assumption in the present context is that the initial system has a homogeneous isothermal core. Young’s models have been widely discussed in the literature, yield definite predictions, and have not previously been compared in detail to HST results for a large sample of galaxies. They are therefore the natural starting point for any investigation. In addition, stellar systems do in fact exist for which the central regions are well approximated by an isothermal sphere. Globular clusters that have not undergone core collapse due to two-body relaxation are observed to have constant density isothermal cores (e.g., Trager, King & Djorgovski 1995). This

³To obtain the appropriate initial state, one merely needs to adiabatically remove the assumed BH from the observed current state. The BH mass cannot be chosen completely arbitrarily if one demands that the initial state is dynamically stable and physically plausible (e.g., has a monotonically decreasing density with radius), but these constraints by themselves are not likely to strongly constrain the BH mass.

may indicate that isothermal cores are a natural attribute of any stellar system. The fact that constant density cores are not found in the centers of early-type galaxies may indicate merely that the density distribution in their nuclear regions has been altered by the presence of a BH, and it is exactly this proposition that will be tested by the present paper.

Young’s models make two strong assumptions about the relation between BHs and galaxy formation. It is assumed that galaxies form and relax before BHs start to grow, and it is assumed that the subsequent BH growth is slow compared to the dynamical time. These assumptions provide a viable scenario (e.g., Murphy, Cohn & Durisen 1991), but are not unique. One alternative is that galaxy and BH formation occur rapidly and simultaneously (e.g., Haehnelt & Rees 1993). Interestingly, Stiavelli (1998) recently showed that galaxy formation around a pre-existing BH, for a given BH mass, leads to a similar end-state as adiabatic growth in a pre-existing homogeneous core. This indicates that the predictions of Young’s models may have a larger range of applicability than strictly indicated by their underlying model assumptions. In particular: (i) a good fit to the data with Young’s models does not necessarily imply that a BH indeed grew adiabatically, or that the galaxy ever had a homogeneous core; and (ii) growth of BHs in galaxies before or during galaxy formation does not necessarily invalidate the predictions of Young’s models.

2.3. Predictions

We define the dimensionless BH mass $\mu \equiv M_{\bullet}/M_{\text{core}}$, where $M_{\text{core}} \equiv \frac{4}{3}\pi\rho_0r_0^3$ is a measure of the mass of the initial isothermal core, and r_0 and ρ_0 are the core radius and central density. The radius of the BH ‘sphere of influence’ is $r_{\bullet} \equiv GM_{\bullet}/\sigma_0^2 = 3\mu r_0$, where σ_0 is the velocity dispersion of the initial isothermal sphere ($\sigma_0^2 = \frac{4}{9}\pi G\rho_0r_0^2$; Binney & Tremaine 1987). The shape of the projected intensity profile after BH growth, $I(r)$, depends only on μ ; the quantities r_0 and ρ_0r_0 determine the radial and intensity scaling. Figure 1 shows $I(r)$ for various values of μ .

Before discussing the implications of the BH growth, it is worth pointing out a peculiar property of the isothermal sphere that is visible in Figure 1. The logarithmic slope of the intensity profile decreases monotonically from zero at asymptotically small radii, to $d \log I/d \log r = -1.40$ at $\log(r/r_0) = 0.34$ (indicated by a vertical dashed line in Figure 1). Here the intensity profile has an inflexion point. The logarithmic slope then *increases* with radius and has the value $d \log I/d \log r = -1$ at asymptotically large radii. In real galaxies the intensity profile generally does not have an inflexion point, and the logarithmic slope is significantly steeper at large radii. In the remaining figures of this paper we replaced the model predictions at $\log(r/r_0) > 0.34$ with a power-law of slope $d \log I/d \log r = -1.40$. This was done for visual purposes only; the actual data-model comparison will always be restricted to radii with $\log(r/r_0) < 0.34$. To model observed profiles at radii with $\log(r/r_0) > 0.34$ would require initial conditions that better reproduce the observed behavior of real galaxies at large radii. This would certainly be useful, but we will argue in Section 4.4 that this will not change the main conclusions of this paper.

Figure 1 shows that the adiabatic BH growth yields the well-known asymptotic slope $I \propto r^{-1/2}$ at small radii. However, this asymptotic behavior does not apply until at least

$\log(r/r_0) \lesssim -2$. This region is generally inaccessible to observations. Core radii do not often exceed $r_0 \approx 3''$ (cf. Section 4 below), for which the $\sim 0.1''$ resolution limit of HST corresponds to $\log(r/r_0) = -1.48$. The logarithmic intensity slope at this radius can either be smaller or larger than the asymptotic slope, depending on the value of μ .

To get a quantitative understanding of the observable properties of the models, we have fitted the predicted intensity profiles in Figure 1 with the so-called ‘nuker-law’ parameterization:

$$I(r) = I_b 2^{\frac{\beta-\gamma}{\alpha}} (r/r_b)^{-\gamma} [1 + (r/r_b)^\alpha]^{-\frac{\beta-\gamma}{\alpha}}. \quad (1)$$

This parameterization has been used successfully to describe the nuclear intensity profiles of a large sample of galaxies (Byun et al. 1996, hereafter B96; F97). The intensity is $I(r) \propto r^{-\gamma}$ at small radii and $I(r) \propto r^{-\beta}$ at large radii, with the transition occurring at the break radius r_b ; the parameter α determines the sharpness of the break, and I_b is the intensity at r_b . The model predictions were fit over the radial range $-1.48 \leq \log(r/r_0) \leq 0.34$ (which is bracketed by the dashed vertical lines in Figure 1), which is a typical range that may be observationally accessible. The fitted profiles are shown as dotted curves. The fit parameters are shown as function of μ in Figure 2.

The most interesting parameter is γ , which measures the slope of the intensity profile at the smallest accessible radii. It increases monotonically with μ , from $\gamma = 0$ for $\mu = 0$ to $\gamma = 1.10$ for $\mu = 3.29$ (the largest μ shown in Figure 1). This spans the entire range of values observed with HST (F97). It may seem remarkable that the slope γ for large values of μ is *steeper* than the slope at asymptotically small radii. The reason for this is that for large values of μ the BH ‘sphere of influence’ exceeds the initial core size. The BH then grows in the region where initially $\rho \propto r^{-2}$, which leads to a steeper intensity profile after BH growth (Quinlan et al. 1995). In fact, when larger values of μ are considered than those plotted in Figures 1 and 2, the slope γ eventually even reaches values in excess of 2. Such models are probably less relevant for real galaxies though, which have $\gamma \lesssim 1.1$.

The parameters r_b and I_b of the nuker-law fit determine the radial and intensity scale of the model. They are of the same order as the scale parameters r_0 and $\rho_0 r_0$ of the initial isothermal sphere, but differ more from these scale parameters as μ grows larger. The parameters α and β of the nuker law determine the shape of the intensity profile at and outside the break radius. The models have $\beta \approx 1.5$, independent of μ , while α varies between $\alpha = 1.6$ and $\alpha = 2.5$, depending on μ . These results are not inconsistent with typical observed values (F97; see also Section 4.4 below).

3. Predictions based on scaling relations

The results presented in Figure 2 show that Young’s models of adiabatic BH growth can in principle generate profiles with similar cusp slopes as observed in either core galaxies or power-law galaxies. In this section we address the question whether this does in fact occur for plausible BH masses, and whether there is a natural explanation for the observed correlation between cusp

slope and luminosity. These questions are addressed in a general sense, using established scaling relations for early-type galaxies. Detailed fits to individual galaxies are presented in Section 4.

3.1. Scaling Relations

Early-type galaxies lie on a plane in the space of their four primary global characteristics, i.e., the effective radius r_{eff} , the average projected intensity inside the effective radius I_{eff} , the velocity dispersion σ and the total luminosity L (Djorgovski & Davis 1987; Dressler et al. 1987). For core galaxies, this so-called fundamental plane has an analog in terms of nuclear properties (Lauer 1985; Kormendy 1985). The relevant quantities are now the break radius r_b and break intensity I_b , instead of r_{eff} and I_{eff} . In the present context we are interested in the dependence of r_b and I_b on luminosity. For the sample of F97:

$$\log r_b = -10.02 + 1.15 \log L; \quad \log I_b = 14.45 - 1.00 \log L, \quad (2)$$

where r_b is in pc, I_b is in the V -band and in units of $L_{\odot} \text{pc}^{-2}$, and L is the total V -band luminosity in L_{\odot} . The RMS scatter around these relations is ~ 0.30 dex and ~ 0.32 dex, respectively. The relations (2) are projections of relations (with smaller scatter) in the four-dimensional (r_b, I_b, σ, L) space.⁴

Core galaxies have cusp slopes $\gamma \lesssim 0.3$. The hypothesis here is that these cusps are due to adiabatic BH growth in isothermal cores. Figure 2 then implies that $\mu \leq 0.11$ for core galaxies. The same figure shows that

$$r_0 \approx 1.25 r_b, \quad \rho_0 r_0 \approx 0.79 \Upsilon I_b, \quad (3)$$

to within 5% and 8%, respectively, for all $\mu \leq 0.11$. The quantity Υ is the V -band mass-to-light ratio of the stellar population, which transforms the observed projected light intensity (I_b) to a projected surface mass density ($\rho_0 r_0$). Combination of equations (2) and (3) yields for the ‘progenitors’ of core galaxies (i.e., before they grew BHs):

$$\log r_0 = -9.92 + 1.15 \log L; \quad \log \rho_0 r_0 = 14.35 - 1.00 \log L + \log \Upsilon. \quad (4)$$

Power-law galaxies have no well-defined breaks, and hence r_b and I_b reduce to fit parameters with little physical significance. As a result, there is no analog to the relations (2) between r_b , I_b and L for power-law galaxies. The hypothesis that we will explore here is that both core galaxies and power-law galaxies evolved from progenitors with isothermal cores, and that the scale radius and density of the progenitor cores of both types of systems obeyed equations (4). This scenario

⁴The global fundamental plane that connects the quantities $(r_{\text{eff}}, I_{\text{eff}}, \sigma, L)$ is effectively a plane in a three-dimensional space, since $L \equiv 2\pi r_{\text{eff}}^2 I_{\text{eff}}$ by definition. However, the relation that connects (r_b, I_b, σ, L) for core galaxies is a relation in a four-dimensional space, since there is no a priori reason why r_b and I_b should uniquely determine L . The slope of the core fundamental plane is not exactly identical to that of the global fundamental plane; e.g., $I_b r_b^2 \propto L^{1.3}$, whereas $I_{\text{eff}} r_{\text{eff}}^2 \propto L$.

predicts for core galaxies and power-law galaxies of the same luminosity that: (i) differences in cusp slope must be due to differences in BH mass; and (ii) there should be no differences in surface brightness at radii $r \gg r_0$, where BHs do not have an impact. The latter prediction can be verified directly. Figure 3 shows as function of luminosity, for each of the galaxies in the sample of Section 4, the observed V -band surface brightness at $r = 5\bar{r}_0$; here \bar{r}_0 is defined to be the progenitor core radius predicted by equation (4). Indeed, core galaxies and power-law galaxies of the same luminosity have the same surface brightness outside the nuclear region. This is partly a restatement of the fact that these galaxies also follow the same set of global fundamental plane relations.

A BH in the center of a galaxy induces a $v \propto r^{-1/2}$ cusp in the rotation velocity or velocity dispersion of a tracer population near the nucleus. High spatial resolution kinematical measurements can therefore yield accurate BH mass determinations for individual galaxies. This area of research has seen much progress in recent years, due to the identification of new suitable tracers (water masers clouds; ionized gas disks), increased spatial resolution (e.g., from HST) and improved modeling techniques. Reviews of the various techniques for kinematical BH detection, and of the current state of knowledge can be found in Kormendy & Richstone (1995), Ford et al. (1998), Richstone (1998), van der Marel (1998) and Ho (1998). The BH masses follow a roughly linear scaling relation between BH mass and galaxy luminosity. For disk galaxies this relation involves the bulge or spheroid luminosity, rather than the total luminosity, but this can be ignored in the present study, which deals exclusively with early-type galaxies. A recent collection of published BH mass estimates yields (van der Marel 1998; see also Figure 8b below):

$$\log M_{\bullet} = -1.96 + 1.00 \log L, \quad (5)$$

with a RMS scatter of ~ 0.59 dex. We will use this relation here, although it remains unclear to what extent this relation may be influenced by selection bias. In particular, there may be a population of galaxies with lower BH masses that have to date remained undetected. Complete samples of kinematically well-studied galaxies are required to test this.

The mass-to-light ratios of early type galaxies have a shallow correlation with luminosity. Axisymmetric dynamical models for spatially resolved kinematical profiles yield (van der Marel 1991; Magorrian et al. 1998, hereafter M98):

$$\log \Upsilon = -1.12 + 0.18 \log L, \quad (6)$$

with a RMS scatter of ~ 0.12 dex.

Combination of equations (4), (5) and (6) yields for the quantity $\mu \equiv M_{\bullet}/(\frac{4}{3}\pi\rho_0r_0^3)$ of the adiabatic BH growth models:

$$\log \mu = 4.03 - 0.48 \log L. \quad (7)$$

A crude estimate for the RMS scatter in this relation is obtained by adding the scatter in the constituent quantities in quadrature (this ignores correlations), which yields 0.80 dex. The absolute magnitude in the V -band, M_V , is related to the luminosity L according to $M_V = 4.83 - 2.5 \log L$, so alternatively:

$$\log \mu = 3.10 + 0.192M_V. \quad (8)$$

3.2. Profile shapes at the distance of the Virgo cluster

Equations (4) and (7) predict r_0 , $\rho_0 r_0$ and μ for any given luminosity L . This allows calculation of the complete surface brightness profile predicted by the adiabatic BH growth scenario, in physical units, for a given luminosity.

As an example we consider the case of galaxies at the distance of the Virgo cluster (the typical distance for most of the galaxies in the F97 sample). Figure 4 shows the predicted profiles for absolute magnitudes $M_V = -22.5, -21.5, \dots, -17.5$. This range of M_V values corresponds roughly to that for the Virgo galaxies in the F97 sample. The values of μ dictated by equation (8) range from $\mu = 0.061$ for $M_V = -22.5$ to $\mu = 0.55$ for $M_V = -17.5$, which is always small enough that the BH growth leaves the profile outside r_0 unaltered. At the distance of the Virgo cluster $\log r_0[\text{arcsec}] = -9.57 - 0.46M_V$, and the initial core radius is below the $\sim 0.1''$ HST resolution limit for all $M_V > -18.63$.⁵ So for $M_V = -17.5$ and $M_V = -18.5$, the profiles before and after BH growth (dashed and solid curves, respectively) are identical and both reflect the adopted initial model outside the core radius (in this case a power law of logarithmic slope -1.40 , see Section 2.3). As the luminosity is increased, the initial core radius r_0 (indicated by a dotted vertical line) shifts into the observable range. The profiles inside r_0 have a power-law cusp, due to the BH. For $M_V = -19.5$ and $M_V = -20.5$, the transition from the outer power-law slope to the inner power-law cusp is shallow enough that these profiles would still be classified in the F97 scheme as power-law profiles, not core profiles. However, the dimensionless BH mass μ , and therefore also the power-law cusp slope γ (cf. Figure 2), decreases with luminosity, whereas r_0 increases with luminosity. These effects combine to produce a pronounced break in the profiles for $M_V = -21.5$ and $M_V = -22.5$, leading them to be classified as core profiles. Figure 4 therefore shows that the models naturally predict a transition from power-law profiles to core profiles with increasing luminosity, as seen in HST observations.

3.3. Comparison to observed cusp properties

For a more quantitative assessment of the model predictions we have fitted nuker-law parameterizations to the profiles predicted for various absolute magnitudes. The most relevant parameters in the present context are the central cusp slope γ and the break radius r_b . These are shown as function of absolute magnitude in Figure 5, using as before the distance of the Virgo cluster. Results are shown not only for the standard BH masses given by equation (5), but also for the cases of BH masses that are three times smaller and three times larger than suggested by this relation, as well as for the no-BH case (which corresponds to the initial isothermal models).

F97 define core galaxies as galaxies that have both $\gamma \leq 0.3$ and $r_b \geq 0.16''$. All other galaxies are classified as power-law galaxies.⁶ F97 find that in general, galaxies with $M_V > -20.5$ have

⁵In fact, at the distance of the Virgo cluster a galaxy with an isothermal core following relation (4) would only be classified as a core galaxy for $M_V > -19.07$; cf. Figure 5 below.

⁶In atypical cases galaxies may have $\gamma \leq 0.3$ and $r_b \geq 0.16''$, yet show no clear break. This can occur when the

power-law profiles, galaxies with $M_V < -22$ have core profiles, and both profile types occur in galaxies with $-22 < M_V < -20.5$. The model predictions presented here are remarkably consistent with these observations. The heavy solid curves in Figure 5 show that models with the standard BH masses of equation (5) predict that galaxies at the distance of Virgo fainter than $M_V = -21.2$ are power-law galaxies, and that galaxies brighter than $M_V = -21.2$ are core galaxies. Both the sense and the absolute magnitude of the predicted transition are the same as observed! The BH masses of galaxies are likely to have an intrinsic scatter, and this naturally explains the observed existence of both power-law galaxies and core galaxies in the region around the transition magnitude.

Both the absence of core galaxies at sufficiently faint luminosities and the absence of power-law galaxies at sufficiently bright luminosities is generically reproduced by the models. However, to reproduce that the cut-offs occur at $M_V = -20.5$ and $M_V = -22$ requires a certain amount of fine-tuning. It is reproduced if there are no galaxies at $M_V > -20.5$ with BH masses smaller than 0.6 times those given by equation (5), and if there are no galaxies at $M_V < -22$ with BH masses larger than 1.5 times those given by equation (5). A situation in which this may occur naturally is if the relation between $\log M_\bullet$ and $\log L$ actually has a somewhat shallower slope than suggested by equation (5). The slope in equation (5) itself is not ruled out, but the cutoffs at $M_V = -20.5$ and $M_V = -22$ are then somewhat surprising given that BH masses inferred from kinematical observations of nearby galaxies have a RMS scatter around equation (5) of a factor ~ 4 . Such a scatter would lead one to expect to find some power-law galaxies at $M_V < -22$ and some core galaxies at $M_V > -20.5$. Instead, the F97 sample contains none of the former; it contains two of the latter (M31 and NGC 4486B), but these are both rather atypical (among other things, both have a double nucleus; Lauer et al. 1993, 1996). Possibly, larger samples will shed more light on the rigidity of the observed cutoffs at $M_V = -20.5$ and $M_V = -22$.

Observations indicate not only that the cusp slopes of early-type galaxies correlate with luminosity, but also that the distribution of cusp slopes is bimodal (Gebhardt et al. 1996; F97; but see Merritt 1997 for an alternative view). The primary evidence for this is a lack of galaxies with $\gamma = 0.4 \pm 0.1$. Observed core galaxies have $\gamma \lesssim 0.3$ and observed power-law galaxies have $\gamma \approx 0.8 \pm 0.3$. This cannot be explained with the present scenario if all galaxies have the same M_\bullet/L given by equation (5), which predicts that galaxies with $-20.0 < M_V < -21.2$ produce cusp slopes $\gamma = 0.4 \pm 0.1$ (cf. Figure 5). Hence, a bimodal distribution in M_\bullet/L is required to reproduce the observed bimodality in γ . For example, assume that there are two populations of galaxies in the luminosity range $-22 < M_V < -20.5$ where core and power-law galaxies overlap: galaxies that have three times smaller BH masses than suggested by equation (5), and galaxies that have three times larger BH masses than suggested by this equation. Figure 5 shows that the former galaxies will all be core galaxies with $\gamma \leq 0.2$ and that the latter will all be power-law galaxies with $\gamma > 0.5$, reproducing the observed bimodality.

Evidence has been mounting in recent years that there are two types of elliptical galaxies:

best nuker-law fit invokes an anomalously low $\alpha \lesssim 0.5$. Examples are NGC 4564 in the F97 sample, and NGC 4589 in the C97 sample. These galaxies are classified as power-law galaxies.

luminous ellipticals with boxy isophotes that are pressure supported by an anisotropic velocity distribution, and small ellipticals with disk-like isophotes that are flattened by rotation. Kormendy & Bender (1996) suggested a formal subdivision of the Hubble sequence based on these criteria. F97 found an almost perfect correspondence between this bimodality in the global properties of elliptical galaxies and the bimodality in the nuclear cusp slopes. Galaxies with disk-like isophotes have power-law profiles and galaxies with boxy isophotes have core profiles. The scenario presented here explains this as a result of higher values of M_{\bullet}/L in disk-like galaxies than in boxy galaxies. The number of galaxies with kinematically determined BH masses is too small at present to either confirm or rule out this hypothesis directly. However, the observed bimodality in both the global and nuclear properties of elliptical galaxies implies that a bimodal distribution of M_{\bullet}/L may not be unnatural. The formation of disk-like galaxies is believed to be characterized by dissipation, either during galaxy formation or at the time of the last major merger. This suggests the presence of large amounts of gas, a significant fraction of which may have been used to form or feed a BH. This provides a plausible reason why M_{\bullet}/L would be larger in disk-like galaxies than in boxy galaxies.

4. Fits to individual galaxies

The results of Section 3 show that the scenario of adiabatic BH growth combined with established scaling relations reproduces the generic nuclear photometric properties of early-type galaxies. However, in any sample of real galaxies one should expect an intrinsic scatter in the relevant model parameters, r_0 , ρ_0 , M_{\bullet} , as well as in distance. So to further address the plausibility of the proposed scenario we proceed by analyzing the surface brightness profiles of individual galaxies.

4.1. Sample selection

The heart of the sample studied here is the F97 sample, which is itself a collection of galaxies from various sources, including Lauer et al. (1995), Jaffe et al. (1994) and various WFPC/GTO programs. To the F97 sample we added those galaxies in B96 and C97 that are not already contained in the F97 sample. From the combined sample we removed the few galaxies that are not classified as an early type (E, E/S0 or S0) in the RC3 (de Vaucouleurs et al. 1991). We removed two more galaxies for which only the profile classification is available (core or power-law), without further information on the surface brightness profile. The resulting sample has 71 galaxies, and contains the majority of the nearby early-type galaxies that have been imaged to date with HST.

BHs with plausible masses do not influence the surface brightness profile at radii $r \gtrsim r_0$, cf. Sections 2 and 3. So to obtain meaningful information for a given galaxy, there must be at least a small radial range $r \lesssim r_0$ for which the surface brightness profile is not degraded by the $\sim 0.1''$ resolution of HST. We therefore removed all galaxies from the sample with $\bar{r}_0 < 0.3''$, where as before \bar{r}_0 is for each galaxy defined to be the progenitor core radius predicted by equation (4). This removes all low-luminosity galaxies with $M_V > -19.7$. For these galaxies one generally

expects to resolve neither a clear signature of a core, nor of a BH (cf. Figure 4).⁷ The remaining sample contains 46 galaxies. Basic properties are listed in Tables 1 and 2, for core and power-law galaxies, respectively.

4.2. Fitting strategy

The surface brightness profiles of early-type galaxies are well fit by the nuker-law parameterization given in equation (1), over the radial range $0.1'' \leq r \leq 10''$. The typical RMS error of a fit is 0.02 mag (B96). Heavy solid curves in Figures 6 and 7 show the nuker laws that best fit the data for all core and power-law galaxies in the sample, respectively. The literature sources of the nuker-law parameters are listed in Tables 1 and 2. C97 present both *V*-band and *I*-band data, but we used only the *V*-band data from their study for consistency with F97 and B96 (which present only *V*-band data). For galaxies contained in the samples of both F97 and C97 we used only the F97 data (but the C97 data yield similar results, see below). The brightness profiles in the figures are shown as function of the mean radius $r = \sqrt{ab}$, where *a* and *b* are the semi-major and semi-minor axes of an elliptical isophote. This choice is most appropriate for comparison to the predictions of our spherical models.

We chose to fit the adiabatic BH growth models to the best-fitting nuker-law parameterizations, rather than to the actual surface brightness data points.⁸ This not only has the advantage of simplicity, but also allows galaxies to be included in the study for which the best-fitting nuker-law parameters have been published, but not the actual surface brightness data points. The accuracy to be gained by fitting the actual data points is only very modest, given how well the data are described by a nuker law. This was verified explicitly for the case of M87, for which the BH mass inferred by fitting to the data directly differs by only 0.04 dex from the BH mass inferred by fitting to the nuker law parameterization.

The non-hatched regions in the panels of Figures 6 and 7 indicate for each galaxy the region over which the models were fit to the data. This region always excludes radii $r < 0.1''$, which are degraded by the HST point-spread function (PSF). It also excludes radii with $\log(r/\bar{r}_0) > 0.3$, for which the surface brightness profile is not expected to be influenced by the possible presence of a BH (cf. Sections 2 and 3). So at these radii one would merely be comparing the initial model to the data, which is meaningless, because no effort was made to find an initial model that accurately represents the large radii behavior of real galaxies. The fit region was never allowed to extend beyond $10''$; the HST data do not typically extend this far, and the nuker-law description of the data breaks down at these radii.

The adiabatic BH growth models have three free parameters: r_0 , which sets the radial scale;

⁷Kinematical detection of BHs in such low-luminosity galaxies is difficult as well. The BH sphere of influence is $r_\bullet \equiv GM_\bullet/\sigma_0^2 = 3\mu r_0$ (cf. Section 2.3). Equations (4) and (7) yield $\log r_\bullet = -5.41 + 0.67 \log L$, so at the distance of the Virgo cluster $r_\bullet < 0.20''$ for all $M_V > -19.7$.

⁸For convenience, we will nonetheless refer to ‘the model fit to the data’.

$\rho_0 r_0 / \Upsilon$, which sets the intensity scale; and μ , which determines the BH mass. The brightness profiles for core galaxies have three well-determined characteristic quantities: r_b , the radius at which a break occurs; I_b , the intensity at that radius; and γ , the inner cusp slope. For core galaxies it is therefore possible to infer a unique best-fitting value for each model parameter. By contrast, the brightness profiles of power-law galaxies have no clear break and no characteristic scale radius. This yields a degeneracy in the modeling, in the sense that models with different r_0 and M_\bullet can provide very similar fits to the data. To break this degeneracy, we assume for power-law galaxies that r_0 is known a priori, and we fix it to the value \bar{r}_0 predicted by equation (4). So for power-law galaxies we merely determine the M_\bullet values implied by the hypothesis that power-law galaxies had progenitor cores that obeyed the same scaling relations as core galaxies, while for core galaxies we actually determine both r_0 and M_\bullet from the data without further assumptions.

A fit to an observed brightness profile yields only the ratio M_\bullet / Υ , not the BH mass M_\bullet itself. To obtain the latter requires knowledge of the stellar mass-to-light ratio Υ , which can only be determined from kinematical data. Where available, Υ was used from M98. For those galaxies not in their sample, Υ was estimated from equation (6).

4.3. Accuracy of the inferred BH masses

Five galaxies in the F97 sample are also contained in the C97 sample. This allows a direct estimate to be obtained of the typical formal errors in the model parameters (which, by definition, are the RMS differences among model parameters determined from independent data sets). This is important, because our approach of fitting to nuker laws rather than to data points precludes use of the normal statistical procedures. For the five galaxies in common to the F97 and C97 samples, the RMS difference in the inferred $\log M_\bullet$ values is 0.09 dex. This includes the combined random errors from both photon noise and image deconvolution, because F97 used Lucy deconvolved images obtained with the First Wide Field and Planetary Camera (WFPC1), while C97 used images obtained with the Second Wide Field and Planetary Camera (which has internal optics to correct for the spherical aberration of the HST primary mirror).

Some of the sample galaxies have minor or patchy dust obscuration. This should have little effect on the inferred BH masses, because the literature sources from which we took the nuker law parameterizations always excluded or corrected for dust regions where necessary. There are no galaxies in the sample with extreme dust absorption across the nucleus, such as NGC 4261 (Ferrarese, Ford & Jaffe 1996) or NGC 7052 (van der Marel & van den Bosch 1998), because F97 rejected such galaxies from their sample.

The effects of additional photometric components in the sample galaxies is more difficult to assess. Out of 16 power-law galaxies in the sample, 4 galaxies have a nuclear stellar cluster and 9 galaxies have a nuclear stellar disk. Such components are not common in core galaxies. Nuclear stellar clusters were always excluded from the fit by the literature sources from which we took the nuker law parameterizations, and they should therefore not bias the BH masses inferred here. However, this remains somewhat speculative as long as the relation between the presence

of a nuclear stellar cluster and a possible BH is unknown. By contrast, none of the literature sources from which we took the nuker law parameterizations corrected for or subtracted nuclear stellar disks. It is not clear whether this would in fact be desirable, but it is certainly useful to know how sensitive the inferred BH mass is to the presence of a stellar disk. The galaxy NGC 4570 has nuclear stellar disk (van den Bosch, Jaffe & van der Marel 1998; van den Bosch & Emsellem 1998; Scorza & van den Bosch 1998), and provides a useful test case in this context. F97 presented the overall best-fitting nuker law for this galaxy, while Scorza & van den Bosch (1998) performed a disk-bulge decomposition and presented only the best-fitting nuker law to the bulge component. When modeled with the scenario presented here, the BH masses implied by the nuker law fits of F97 and Scorza & van den Bosch differ by 0.19 dex. This is consistent with the arguments presented in both papers that nuclear stellar disks are not the cause of the steep cusps in power-law galaxies, and suggests that nuclear stellar disks are not a major source of uncertainty in the BH masses inferred here for power-law galaxies.

So the overall uncertainty in the inferred BH masses due to photon noise, PSF deconvolution, dust, nuclear stellar clusters and nuclear stellar disks is 0.2–0.3 dex. Tables 1 and 2 show that the models invoke a BH to fit the data for all galaxies, and this small error estimate suggests that these detections are highly significant (given the model assumptions). One may nonetheless wonder whether there are some galaxies in our sample for which the models may also be consistent with the data for $M_{\bullet} = 0$. Gebhardt et al. (1996) studied non-parametric deprojections of the surface brightness profiles of a large sample of early-type galaxies observed with HST. A total of 24 galaxies from our sample of 46 are included in their sample. In only two of these galaxies (NGC 1600 and NGC 4889) can the existence of an isothermal core not be excluded at the $0.1''$ resolution limit of HST. If these statistics are representative for our sample as a whole, then we may expect that the models could be consistent with $M_{\bullet} = 0$ for ~ 4 galaxies in our sample of 46. This is small enough not to influence the conclusions in the following sections on the overall properties of the sample.

4.4. Fit results

Dashed curves in Figures 6 and 7 show the best model fits to the data for all galaxies. Dotted curves show the isothermal profiles before BH growth. The parameters of the best-fitting models are listed in Tables 1 and 2.

Figure 6 shows the core galaxies in the sample. The brightness profiles for these galaxies are generally well fit by the models; the average RMS residual is only $0.03 \text{ mag/arcsec}^2$. In some galaxies, the models fit the data even outside the region where the fit was performed (the hatched region); examples are A1020, NGC 720, and IC 1459. However, this is not generally true, as witnessed by, e.g., A2052, NGC 524 and NGC 4168. This is because outside the break radius r_b , real galaxies show a larger variety of properties than the models. The nuker-law parameter β measures the intensity profile slope outside r_b , and α determines the sharpness of the break. The core galaxies in the sample have rather broad distributions of α and β . The 16% and 84% percentiles for α are 0.90 and 3.57; for β they are 1.05 and 1.64. By contrast, the models for

core galaxies always have $\alpha = 2.3 \pm 0.1$ and $\beta = 1.55 \pm 0.1$ (cf. Figure 2 for $\mu \leq 0.11$, $\gamma \leq 0.3$). This is because outside r_b they always resemble the isothermal sphere. With more general initial conditions it should be possible to fit the observed profiles of core galaxies also outside the break radius r_b . In particular, one could study initial conditions with homogeneous cores but a larger variety of outer profile properties. We have not explored this, because the resulting BH masses would probably not be very different. The properties of the initial model at $r \gtrsim r_0$ have little influence on the predicted distribution after BH growth at $r \lesssim r_0$, unless the size r_\bullet of the BH sphere of influence actually extends significantly into the region $r > r_0$. This is not the case, since $r_\bullet = 3\mu r_0$, and $\mu < \frac{1}{3}$ for the large majority of the galaxies in the sample.

Figure 7 shows the power-law galaxies in the sample. The fits for these galaxies are somewhat poorer than for the core galaxies, due in part to the fact that r_0 was fixed a priori (so that one less free parameter is available to optimize the fit). The average RMS residual is 0.08 mag/arcsec². The mismatch is typically in the sense that the predicted profiles have slightly more curvature than the observed profiles. However, the fits are still reasonable, given the simple nature of the models. There are a few galaxies for which the fit is acceptable even outside the fit-region, e.g., NGC 1439 and NGC 3377, but these are exceptions. More typically, the predictions fall below the observations at large radii. As for core galaxies, this can probably be improved with a more general choice of initial conditions.

Overall, the fits to the HST photometry are quite acceptable, especially for core galaxies and somewhat less so for power-law galaxies. However, the main test of the proposed scenario is not whether individual profiles can be well fit, but rather whether the required BH masses are plausible. Based on the general discussion in Section 3 we already expect this to be the case, but this can now be tested in detail.

4.5. The BH mass distribution

Figure 8a shows the BH masses for all 46 sample galaxies as function of the V -band luminosity L . Pearson’s linear correlation coefficient $r = 0.68$ indicates a statistically significant correlation between $\log M_\bullet$ and $\log L$. The dashed line is the best linear least-squares fit for the sample as a whole,

$$\log M_\bullet = 0.76 + 0.75 \log L. \quad (9)$$

The slope of this line is somewhat smaller than unity, but this is not highly significant given the limited $\log L$ range of the sample (the formal error on the inferred slope is 0.12). The RMS scatter around the fit is 0.31 dex. The solid line is the best-fitting line of unit slope

$$\log M_\bullet = -1.83 + 1.00 \log L, \quad (10)$$

for which the RMS scatter is 0.33 dex.

Figure 8b shows a collection of kinematical BH detections in nearby galaxies (adapted from van der Marel 1998, with NGC 7052 added from van der Marel & van den Bosch 1998). The long-dashed line is the relation given by equation (5). In Section 3.3 we showed that many of the

photometric properties of early-type galaxies observed with HST are consistent with the presence of BHs with masses following equation (5). A comparison of Figure 8a and 8b now confirms this directly. The BH mass distribution implied by the adiabatic BH growth models is consistent with that determined kinematically. The difference between equations (5) and (10) is only 0.13 dex, significantly smaller than the RMS scatter in either relation.

Several other suggestions from Section 3.3 are neither strongly confirmed nor strongly disproved here. First, it was argued that power-law galaxies should have higher BH masses than core galaxies, at a given luminosity. We find here that the core galaxies in the sample have $\langle \log(M_{\bullet}/L) \rangle = -1.91$ with a RMS scatter of 0.29, whereas the power-law galaxies have $\langle \log(M_{\bullet}/L) \rangle = -1.68$ with a RMS scatter of 0.34. So on average power-law galaxies do have larger BH masses than core galaxies, but the difference is not highly significant (the errors on the mean $\langle \log(M_{\bullet}/L) \rangle$ are 0.05 dex and 0.09 dex, respectively). Second, it was argued from the observed absence of core galaxies at $M_V > -20.5$ and the observed absence of power-law galaxies at $M_V < -22$ that the relation between $\log M_{\bullet}$ and $\log L$ may have a slope less than unity. This is confirmed by equation (9), but again not at high significance. Third, it was argued that the absence of galaxies with intermediate slope brightness profiles may indicate a bimodality in the BH mass distribution. Figure 8a shows that core galaxies and power-law galaxies do tend to occupy somewhat different regions in the (M_{\bullet}, L) plane, but there does not seem to be a very clear bimodality. In particular, there is a region around $\log L = 10.3$ ($M_V = -20.9$) and $\log M_{\bullet} = 8.6$ in which the two types of galaxies overlap.

4.6. Kinematically determined BH masses for individual galaxies

The accuracy of the photometrically determined BH masses, $M_{\bullet, \text{adi}}$, can be further assessed by studying individual galaxies with kinematically determined BH masses. Four galaxies in the sample have securely determined BH masses, $M_{\bullet, \text{sec}}$, from HST spectroscopy (cf. Figure 8b), namely: NGC 3115 (Kormendy et al. 1996), NGC 3377 (Kormendy et al. 1998; Richstone 1998), NGC 3379 (Gebhardt et al. 1998) and NGC 4486 (=M87; Harms et al. 1994; Macchetto et al. 1997). These BH mass determinations are typically believed to be accurate to $|\log \Delta M_{\bullet, \text{sec}}| \lesssim 0.3$. Figure 9a compares the photometrically and kinematically determined BH masses for these four galaxies. The agreement is very good: on average $\langle \log(M_{\bullet, \text{adi}}/M_{\bullet, \text{sec}}) \rangle = 0.19$ with a RMS scatter of 0.25 dex. The agreement is no poorer for power-law galaxies than for core galaxies. NGC 3115 has both a nuclear stellar cluster and a nuclear stellar disk, so the agreement for this galaxy strengthens the arguments of Section 4.3 that these components do not bias the BH mass estimate. Overall, the results in Figure 9a provide additional credibility to the interpretation of observed surface brightness cusps in both core galaxies and power-law galaxies as due to adiabatic BH growth in initially isothermal cores. Unambiguous detection of BHs in individual galaxies will always require high spatial resolution kinematical data, but Figure 9a shows that it is justified to use photometrically determined BH masses such as those in Tables 1 and 2 as a useful guide when such kinematical data are not available.

The other galaxies in Figure 8b with kinematically determined BH masses do not pass the

criteria of our sample, despite the fact that HST photometry is available for some of them. We briefly discuss these galaxies in Appendix A, and present some detailed model fits for M32. The results for M32 are not inconsistent with those presented here for the main sample.

M98 analyzed ground-based stellar kinematical observations of a large sample of early-type galaxies using stellar dynamical models with phase-space distribution functions of the form $f(E, L_z)$. These models can be viewed as the axisymmetric generalizations of spherical isotropic models. M98 showed that most of the galaxies in their sample must have BHs if these distribution functions are correct. However, it is unknown whether real galaxies do in fact have isotropic velocity distributions. The range of possible velocity anisotropies in equilibrium systems is large (e.g., Statler 1987), and any anisotropy may have a significant impact on the inferred mass distribution (Binney & Mamon 1982). So the accuracy of the inferred BH masses is determined entirely by the unknown accuracy of the underlying model assumptions, as is the case for our photometric models. Our sample has 21 galaxies in common with the sample of M98. Figure 9b compares the photometrically determined BH masses for these galaxies to the values $M_{\bullet, \text{iso}}$ implied by the $f(E, L_z)$ models. The BH masses agree reasonably well for nearby galaxies with distances $D < 30$ Mpc (i.e., twice the distance of the Virgo cluster): on average $\langle \log(M_{\bullet, \text{adi}}/M_{\bullet, \text{iso}}) \rangle = -0.09$ with a RMS scatter of 0.41 dex. However, the results for galaxies with $D > 30$ Mpc disagree by an order of magnitude: $\langle \log(M_{\bullet, \text{adi}}/M_{\bullet, \text{iso}}) \rangle = -0.93$ with a RMS scatter of 0.42 dex. The isotropic kinematical models require larger BH masses than the photometric models. The galaxies at $D > 30$ Mpc are all core galaxies; if they have the massive BHs suggested by M98, then our models predict much steeper brightness cusps than observed. Van der Marel (1998) showed that this discrepancy can be resolved by assuming that core galaxies have mild radial velocity anisotropy, either throughout the galaxy or only outside the core region (for the case of an isotropic core). Such radial anisotropy would be consistent with several detailed studies of core galaxies (van der Marel 1991; Bender, Saglia & Gerhard 1994; Merritt & Oh 1997; Rix et al. 1998; Gerhard et al. 1998; Gebhardt et al. 1998), and could be due, e.g., to violent relaxation during dissipationless galaxy formation (van Albada 1982). Radial anisotropy would cause isotropic models to overestimate the BH mass (or invoke a BH when there is none). The BH masses inferred from isotropic models would be most in error for distant galaxies, for which the BH sphere of influence would be smaller than the spatial resolution of ground-based kinematical observations. A BH mass overestimate of a factor 10 for a distant galaxy does not require an implausibly large velocity anisotropy, as was shown by van der Marel (1998) for the case of NGC 1600 ($D = 50$ Mpc).

4.7. Model parameters

In Section 3.1 we derived scaling relations for the parameters of the adiabatic BH growth models. These can now be verified with the results obtained for individual galaxies. Figure 10 shows the inferred parameters, i.e., the progenitor core radius r_0 , the progenitor core intensity scale $\rho_0 r_0 / \Upsilon$, and the dimensionless BH mass μ , for all sample galaxies as function of luminosity. The solid lines are the predicted scaling relations from equations (4) and (7).

The inferred values for r_0 and $\rho_0 r_0 / \Upsilon$ closely follow the predicted relations (but remember

that for power-law galaxies r_0 was fixed a priori). The inferred values of μ are higher for power-law galaxies than for core galaxies, in agreement with the predictions of Section 3. However, the inferred values show a somewhat steeper dependence on luminosity than predicted by equation (7). This is because the latter equation is based on the assumed linear dependence between M_\bullet and L from equation (5), while it was shown in Section 4.5 that the inferred BH masses imply a somewhat shallower slope. The long-dashed line in the right panel of Figure 10 shows the prediction obtained by combining equations (4) and (6) with equation (9). This line does reproduce the trend in the inferred μ values adequately. Overall, the results for individual galaxies validate the more general analysis of Section 3.

5. Concluding remarks

5.1. Summary

We have studied a scenario for the nuclear structure of early-type galaxies based on the assumption that galaxies have central BHs that grew adiabatically in homogeneous isothermal cores, as first proposed by Young (1980), and we have compared the predictions of this scenario to the nuclear properties of early-type galaxies observed with HST. The models reproduce and explain many of the observed nuclear photometric properties of early-type galaxies remarkably well. The main results are the following.

1. The models can fit the full range of cusp slopes found at the smallest radii observable with HST, $I \propto r^{-\gamma}$ with $0 \leq \gamma \lesssim 1.1$, despite the fact that the models always predict $I \propto r^{-1/2}$ at asymptotically small radii. The cusp slope at observable radii is determined by the dimensionless BH mass, $\mu = M_\bullet/M_{\text{core}}$, where $M_{\text{core}} \equiv \frac{4}{3}\pi\rho_0r_0^3$ is a measure of the mass of the ‘progenitor’ core. Models with larger μ yield larger cusp slopes γ .
2. ‘Core galaxies’ have surface brightness profiles with a clear break, inside which $\gamma \leq 0.3$. The break radius r_b and break surface brightness I_b obey scaling relations similar to those of the fundamental plane. The cusp slopes in these galaxies can be explained as the result of BHs with small values of μ : $\mu \lesssim 0.1$. The quantities r_b and I_b in models with small μ reflect the core radius r_0 and scale intensity ρ_0r_0 of the progenitor core (with proportionality constants of order unity). So the observed scaling relations for r_b and I_b are due to scaling relations that governed the properties of the homogeneous progenitor cores.
3. ‘Power-law galaxies’ are galaxies with $\gamma > 0.3$. Their surface brightness profiles have no clear break, and there are no characteristic radius and intensity for these galaxies that obey scaling relations similar to those for core galaxies. The steep cusps and absence of a break in these galaxies can be explained as the result of BHs with $\mu \gtrsim 0.1$. It is attractive to assume that the progenitor cores of power-law galaxies obeyed the same scaling relations as the progenitor cores of core galaxies. This is plausible in view of the fact that power-law galaxies and core galaxies also follow the same fundamental plane relations, and it is consistent with observed brightness profiles outside the central region.

4. At the small radii of interest, the surface brightness profiles of individual galaxies are well fit by the models. To fit the data at all radii requires models with more realistic initial conditions at large radii. The inferred BH mass distribution for a sample of 46 galaxies with available HST photometry suggests a roughly linear correlation between BH mass and V -band galaxy luminosity, of the form $\log M_{\bullet} \approx -1.83 + \log L$ (RMS scatter 0.33 dex). This agrees with the average relation for the 18 nearby galaxies with kinematically well-determined BH masses, to within 0.13 dex (much better than RMS scatter in either relation). For the four galaxies in common to both samples, the individually determined BH masses agree to within ~ 0.25 dex RMS.
5. In general, galaxies with $M_V < -22$ are observed to have core profiles and galaxies with $M_V > -20.5$ are observed to have power-law profiles. Both profile types are found in galaxies with $-22 < M_V < -20.5$. In the models, two effects influence the predicted brightness profile as function of luminosity. First, the core mass M_{core} increases more steeply with luminosity, $M_{\text{core}} \propto L^{1.5}$ (F97), than does the BH mass, $M_{\bullet} \propto L$. Hence, $\mu \propto L^{-0.5}$, so that lower luminosity galaxies are predicted to have steeper cusp slopes.⁹ Second, the core radius r_0 decreases with decreasing luminosity (F97), such that any break present is more difficult to observe in low-luminosity galaxies. At the distance of the Virgo cluster, the models predict core profiles for $M_V < -21.2$ and power-law profiles for $M_V > -21.2$, for galaxies that obey all scaling relations without intrinsic scatter. This naturally reproduces both the sense and the absolute magnitude of the observed transition. Intrinsic scatter in the characteristic quantities r_0 , $\rho_0 r_0$ and M_{\bullet} can explain why both types of galaxies are observed in the region around the transition magnitude.
6. Observations indicate a bimodality between core galaxies and power-law galaxies. The former have $\gamma \leq 0.3$ and the latter have $\gamma = 0.8 \pm 0.3$, with few galaxies showing intermediate slopes, $\gamma = 0.4 \pm 0.1$. This bimodality correlates with the bimodality in the global properties of elliptical galaxies. Core galaxies are luminous, have boxy isophotes and are pressure supported by an anisotropic velocity distribution; power-law galaxies are less luminous, have disky isophotes and are flattened by rotation. The scenario presented here explains the observed bimodality in cusp slopes as a result of higher values of M_{\bullet}/L in disky galaxies than in boxy galaxies. The presence of gas and dissipation during the formation or last major merger of disky galaxies may provide a natural explanation for this.

5.2. Discussion

The scenario presented here is not unique. Observed surface brightness cusps can be interpreted in many different ways, as stressed in Section 1. For example, the observed cusps may have formed dissipationally during galaxy formation, and may not have any relation to BHs at

⁹M98 suggest that $M_{\bullet} \propto M = \Upsilon L \propto L^{1.18}$, cf. equation (6). This implies $\mu \propto L^{-0.32}$, which does not significantly alter the argument presented here.

all. Our scenario is also oversimplified in that it ignores the important issue of accretion events and mergers between galaxies, which will almost certainly alter the brightness profiles of the constituent galaxies (F97). Nonetheless, the proposed scenario naturally predicts observational results that would otherwise remain unexplained (e.g., the correlation between cusp slope and luminosity), and it yields BH masses that agree with those determined kinematically. These findings single out the present scenario as a very attractive one among many possible ones, but it remains surprising that such a simple scenario would work so well.

The success of Young’s scenario does not teach us much about the processes of BH and galaxy formation, and their connection. Even if the surface brightness profiles predicted by the models for a given BH mass are correct, this still does not imply that the BHs in galaxies must have grown adiabatically, or that there ever were progenitor systems with homogeneous cores. Stiavelli (1998) showed that violent relaxation of stars around a pre-existing BH yields a similar end-state as do the models of Young (1980). A wide variety of scenarios in which BHs form before, during, or after the galaxies in which they reside, may therefore all lead to a similar end-state. In fact, this may well be the key to explaining why Young’s models fit the observations so well, despite their apparent simplicity.

If galaxies did in fact start out with homogeneous cores, this still leaves open the questions why these homogeneous cores formed in the first place, and why they followed the scaling relations of equation (4). However, the scenario discussed here does resolve one puzzling issue. It explains through the presence of BHs why the observed nuclear properties of core galaxies follow relations like those of the fundamental plane, whereas the observed nuclear properties of power-law galaxies don’t. This reduces the search for understanding of the global and nuclear parameter relations of galaxies to a single problem, and suggests that our understanding of the global fundamental plane relations of early-type galaxies (e.g., Bender, Burstein & Faber 1992; Burstein et al. 1997) applies to the nuclear parameter relations as well. For example, the fact that the inferred progenitor cores of low-luminosity galaxies are smaller and denser than those of high-luminosity galaxies can probably be attributed to dissipation during galaxy formation (F97 and references therein).

Possibly most importantly, the results in this paper provide strong new support to the hypothesis that all galaxies have BHs, and that BH masses scale approximately with galaxy luminosity according to equations (5) or (10). This remains difficult to prove in a model independent way, but is also indicated by several other studies of active and quiescent galaxies (e.g., Kormendy & Richstone 1995; M98; Ho 1998). It is also consistent with quasar statistics (Sołtan 1982; Chokshi & Turner 1992; F97). If every galaxy spheroid harbors a BH that was formed in a quasar phase through matter accretion with efficiency ϵ , then equation (10) implies that $\epsilon = 0.04$ (van der Marel 1998).

I thank Gerry Quinlan for kindly allowing me to use his adiabatic BH growth software, and Tim de Zeeuw and Marcella Carollo for a careful reading of the manuscript. This work was supported by an STScI Fellowship, awarded by the Space Telescope Science Institute which is operated by the Association of Universities for Research in Astronomy, Incorporated, under NASA contract NAS5-26555.

A. Galaxies with kinematically determined BH masses

Only four of the galaxies with kinematically determined BH masses in Figure 8b are part of the photometric sample discussed in Section 4, namely NGC 3115, NGC 3377, NGC 3379 and NGC 4486 (=M87). The other 14 galaxies do not pass the selection criteria of the sample discussed in Section 4.1.

Our own Galaxy, M31, NGC 1068, NGC 4258, NGC 4594 and NGC 4945 are not early-type galaxies. Apart from this, no HST photometry has been published for NGC 4594 (Sombrero), while dust obscuration is a significant problem in NGC 1068, NGC 4258 and NGC 4945. A useful surface brightness profile is available only for M31, but there the presence of a double nucleus (Lauer et al. 1993) prevents a meaningful comparison between our models and the observed surface brightness profile. The galaxies M84, NGC 4261, NGC 7052 and NGC 6251 are elliptical galaxies, but they all have pronounced dust disks across the nucleus. The rotation velocities of the ionized gas in these disks have yielded the BH mass determinations for these galaxies, but the dust prevents a reliable determination of the stellar brightness profile. For Arp 102B no HST imaging has been obtained to date.

This leaves M32, NGC 4342 and NGC 4486B, for which good HST surface brightness profiles are available. These galaxies are not part of our photometric sample because they have $\bar{r}_0 < 0.3''$ (where \bar{r}_0 is the progenitor core radius predicted by eq. [4]). Specifically, $\bar{r}_0 = 0.22''$ for M32, $\bar{r}_0 = 0.09''$ for NGC 4342 and $\bar{r}_0 = 0.03''$ for NGC 4486B. Thus, if these galaxies follow the scaling relations of Section 3, one expects to resolve neither a clear signature of a core, nor of a BH. The fact that BHs have in fact been detected kinematically implies that these galaxies apparently do not follow the scaling relations obeyed by other galaxies. For M32 and NGC 4342 we discuss this in some detail below. The case of NGC 4486B was already discussed by F97. This satellite galaxy of M87 has a brightness profile with a core, despite its low luminosity ($M_V = -17.57$). F97 suggest that it was once more massive, but was stripped of mass through interaction with M87. NGC 4486B also has a closely separated double nucleus (Lauer et al. 1996), which prevents any meaningful comparison between our models and the observed surface brightness profile.

A.1. M32

M32 is especially interesting in the present context because Lauer et al. (1992b) showed that HST photometry for M32 can be adequately interpreted in terms of Young’s adiabatic BH growth models. M32 is classified by F97 as a power-law galaxy. In general we have used the approach for power-law galaxies of fixing r_0 to the value predicted by equation (4) when doing the adiabatic BH growth model fit. However, the predicted $\bar{r}_0 = 0.22''$ may not be appropriate for M32. The scaling relation in equation (4) is based on the core galaxies in our sample, which span the luminosity range $10.15 \leq \log L \leq 11.35$. By contrast, M32 has $\log L = 8.57$. Small uncertainties in the slope of equation (4) therefore translate to large uncertainties in the predicted r_0 for M32. Based on these considerations we have done a model fit for M32 in which r_0 was not fixed a priori, but was varied to optimize the fit. The fit itself was done over the range of radii with $r \geq 0.1''$ and

$\log(r/r_0) < 0.3$, where the upper limit of the fit range was adjusted iteratively during the fit.

The best fit is shown in Figure 11; its parameters are listed in Table 3. The inferred BH has $\log M_\bullet = 6.68$, which agrees with the kinematically determined value $M_\bullet = 6.59$ (from van der Marel et al. 1998, modified to the same distance used here) to within 0.09 dex. This agreement is similar as for the galaxies with kinematically well-determined BH masses shown in Figure 9. The value of M_\bullet/L for M32 is not atypical, and falls exactly on the relation of equation (5). However, the best-fit model has $r_0 = 0.81''$, which exceeds the prediction of equation (4) by 0.57 dex. This is approximately twice the RMS scatter around equation (4) for core galaxies, insufficient to provide strong evidence that the progenitor core of M32 violates the scaling relations inferred for higher-luminosity galaxies. First, the discrepancy is only at the $\sim 2\sigma$ level; second, uncertainties in the slope of equation (4) may have exaggerated the discrepancy; and third, the luminosity of M32 may have decreased over time due to interactions with M31, with resulting stripping of material. Overall, the results for M32 are not inconsistent with the general scenario discussed in the context of our main sample.

A.2. NGC 4342

NGC 4342 is an S0 galaxy in Virgo with a nuclear stellar disk (van den Bosch et al. 1998; Scorza & van den Bosch 1998). It has a power-law brightness profile, as expected for its luminosity ($M_V = -18.49$). NGC 4342 violates the scaling relations of Section 3 by having an anomalously large M_\bullet/L . Cretton & van den Bosch (1998) use HST stellar kinematics to derive $M_\bullet = 3.0 \times 10^8 M_\odot$. This yields $\log M_\bullet/L = -0.63$, which exceeds the average relation in equation (5) by 1.33 dex. This contrasts with the case of M32, which has a ‘normal’ M_\bullet/L , but a larger r_0 than expected.

To model the NGC 4342 surface brightness profile one would like to assume that it had a progenitor core obeying equation (4), i.e., $r_0 = 0.09''$, but that it somehow grew an anomalously large BH. Interpretation of the observed brightness profile then requires an adequate model of BH growth that influences the region *outside* the homogeneous progenitor core. For this one needs an initial model that reproduces the large radii behavior of real galaxies. As discussed in Section 2.3, the isothermal sphere is not sufficient for this. Young’s models therefore do not allow us to address whether or not NGC 4342 is consistent with the adiabatic BH growth scenario.

REFERENCES

- Bahcall, J. N., & Wolf R. A. 1976, ApJ, 209, 214
- Bahcall, J. N., & Wolf R. A. 1977, ApJ, 216, 883
- Bender, R., Burstein, D., & Faber, S. M., 1992, ApJ, 399, 462
- Bender, R., Saglia, R. P., & Gerhard, O.E. 1994, MNRAS, 269, 785
- Binney, J., & Mamon, G. A. 1982, MNRAS, 200, 361
- Binney, J., & Tremaine, S. 1987, Galactic Dynamics (Princeton: Princeton University Press)
- Burstein, D., Bender, R., Faber, S. M., & Nolthenius, R. 1997, AJ, 114, 1365
- Byun, Y.-I., et al. 1996, AJ, 111, 1889 (B96)
- Carollo, C. M., Franx, M., Illingworth, G. D., & Forbes D. A. 1997, ApJ, 481, 710 (C97)
- Chokshi, A., & Turner, E. L. 1992, MNRAS, 259, 421
- Cipollina, M. 1995, A&AS, 110, 155
- Cipollina, M., & Bertin, G. 1994, A&A, 288, 43
- Crane P., et al. 1993, AJ, 106, 1371
- Cretton, N., & van den Bosch, F. C. 1998, ApJ, submitted [astro-ph/9805324]
- de Vaucouleurs, G., de Vaucouleurs, A., Corwin, H. G., Buta, R. J., Paturel, G., & Fouqué, P. 1991, Third Reference Catalogue of Bright Galaxies (New York: Springer)
- Djorgovski, S., & Davis, M. 1987, ApJ, 313, 59
- Dressler, A., Lynden-Bell, D., Burstein, D., Davies, R. L., Faber, S. M., Terlevich, R., & Wegner, G. 1987, ApJ, 313, 42
- Faber, S. M., et al. 1997, AJ, 114, 1771 (F97)
- Fabian, A. 1997, Astronomy & Geophysics, 38/4, 10
- Ferrarese, L., Ford H. C., & Jaffe W. 1996, ApJ, 470, 444
- Forbes, D. A., Franx, M., & Illingworth, G. D. 1995, AJ, 109, 1988
- Ford, H. C., Tsvetanov, Z. I., Ferrarese L., & Jaffe W. 1998, in Proceedings IAU Symposium 184 (Dordrecht: Kluwer Academic Publishers), in press [astro-ph/9711299]
- Gebhardt, K., et al. 1996, AJ, 112, 105
- Gebhardt, K., et al. 1998, AJ, submitted
- Gerhard, O. E., Jeske, G., Saglia, R. P., & Bender, R. 1998, MNRAS, 295, 197
- Haehnelt, M. G., & Rees, M. J. 1993, MNRAS, 263, 168
- Harms, R. J., et al. 1994, ApJ, 435, L35
- Ho, L. 1998, in Observational Evidence for Black Holes in the Universe, ed. S. K. Chakrabarti (Dordrecht: Kluwer Academic Publishers), in press [astro-ph/9803307]

- Jaffe, W., Ford, H. C., O'Connell, R. W., van den Bosch, F. C., & Ferrarese, L. 1994, *AJ*, 108, 1567
- Kormendy, J. 1985, *ApJ*, 295, 73
- Kormendy, J., & Richstone, D. 1995, *ARA&A*, 33, 581
- Kormendy, J., & Bender, R. 1996, *ApJ*, 464, L119
- Kormendy, J. et al., 1996, *ApJ*, 459, L57
- Kormendy, J., Bender, R., Evans, A., & Richstone, D. 1998, *AJ*, in press [astro-ph/9803307]
- Lauer, T. R. 1985, *ApJ*, 292, 104
- Lauer, T. R., et al. 1992a, *AJ*, 103, 703
- Lauer, T. R., et al. 1992b, *AJ*, 104, 552
- Lauer, T. R., et al. 1993, *AJ*, 106, 1436
- Lauer, T. R., et al. 1995, *AJ*, 110, 2622
- Lauer, T. R., et al. 1996, *ApJ*, 471, L79
- Lee, M. H., & Goodman, J. 1989, *ApJ*, 343, 594
- Macchetto, F., Marconi, A., Axon D. J., Capetti, A., & Sparks W. 1997, *ApJ*, 489, 579
- Magorrian, J., et al. 1998, *AJ*, submitted [astro-ph/9708072] (M98)
- Merritt, D. 1997, in *The Nature of Elliptical Galaxies, Proceedings of the Second Stromlo Symposium*, eds. Arnaboldi, M., da Costa G., & Saha, P. (ASP), 32
- Merritt D., & Oh S. P. 1997, *AJ*, 113, 1279
- Mihos, C. J., & Hernquist, L. 1994, *ApJ*, 437, L47
- Murphy, B. W., Cohn, H. N., & Durisen, R. H. 1991, *ApJ*, 370, 60
- Nakano, T., & Makino, J. 1997, preprint [astro-ph/9710135]
- Navarro, J. F., Frenk, C. S., & White, S. D. M. 1996, *ApJ*, 462, 563
- Peterson, B. M. 1997, *An Introduction to Active Galactic Nuclei* (Cambridge: Cambridge University Press)
- Quinlan, G. D., Hernquist, L., & Sigurdsson, S. 1995, *ApJ*, 440, 554
- Quinlan, G. D., & Hernquist, L. 1997, *New Astronomy*, submitted [astro-ph/9706298]
- Rauch, K. P., & Tremaine, S. 1996, *New Astronomy*, 1, 149
- Richstone, D. 1998, in *Proceedings IAU Symposium 184* (Dordrecht: Kluwer Academic Publishers), in press
- Rix H.-W., de Zeeuw P. T., Cretton N., van der Marel R. P., Carollo, C. M. 1997, *ApJ*, 488, 702
- Scorza, C., & van den Bosch, F. C. 1998, *MNRAS*, submitted [astro-ph/9806078]
- Sigurdsson, S., Hernquist, L., & Quinlan, G. D. 1995, *ApJ*, 446, 75

- Sołtan, A. 1982, MNRAS, 200, 115
- Statler, T. S. 1987, ApJ, 321, 113
- Stiavelli, M. 1998, ApJ, 495, L91
- Trager, S. C., King, I. R., & Djorgovski, S. 1995, AJ, 109, 218
- van Albada, T. S. 1982, MNRAS, 201, 939
- van den Bosch, F. C., Jaffe, W., & van der Marel, R. P. 1998, MNRAS, 293, 343
- van den Bosch, F. C., & Emsellem, E. 1998, MNRAS, in press [astro-ph/9804039]
- van der Marel, R. P. 1991, MNRAS, 253, 710
- van der Marel, R. P. 1998, in Proceedings IAU Symposium 186 (Dordrecht: Kluwer Academic Publishers), in press [astro-ph/9712076]
- van der Marel, R. P., & van den Bosch, F. C. 1998, AJ, submitted [astro-ph/9804194]
- van der Marel, R. P., Cretton, N., de Zeeuw, P. T., & Rix, H.-W. 1998, ApJ, 493, 613
- Young, P. 1980, ApJ, 242, 1232
- Young, P., Westphal, J. A., Kristian, J., Wilson, C. P., & Landauer, F. P. 1978, ApJ, 221, 721

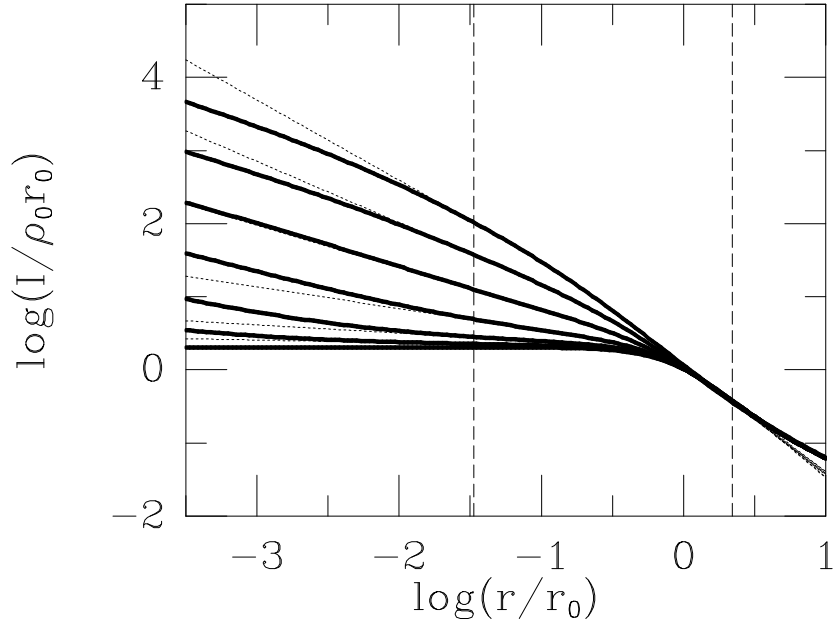


Fig. 1.— Heavy solid curves are the predicted intensity profiles $I(r)$ for models of adiabatic BH growth in an isothermal sphere. The dimensionless BH mass for the models is, from bottom to top, $\mu = 0, 0.011, 0.034, 0.11, 0.34, 1.05$ and 3.29 , respectively. The rightmost of the two dashed vertical lines marks the radius at which the initial model has an inflexion point. The other dashed vertical line marks the radius that corresponds to the $0.1''$ resolution limit of HST for a case in which $r_0 = 3''$. Dotted curves are nuker laws fitted to the models over the radial range between the vertical lines. The quantities r_0 and ρ_0 are the core radius and central density of the initial model.

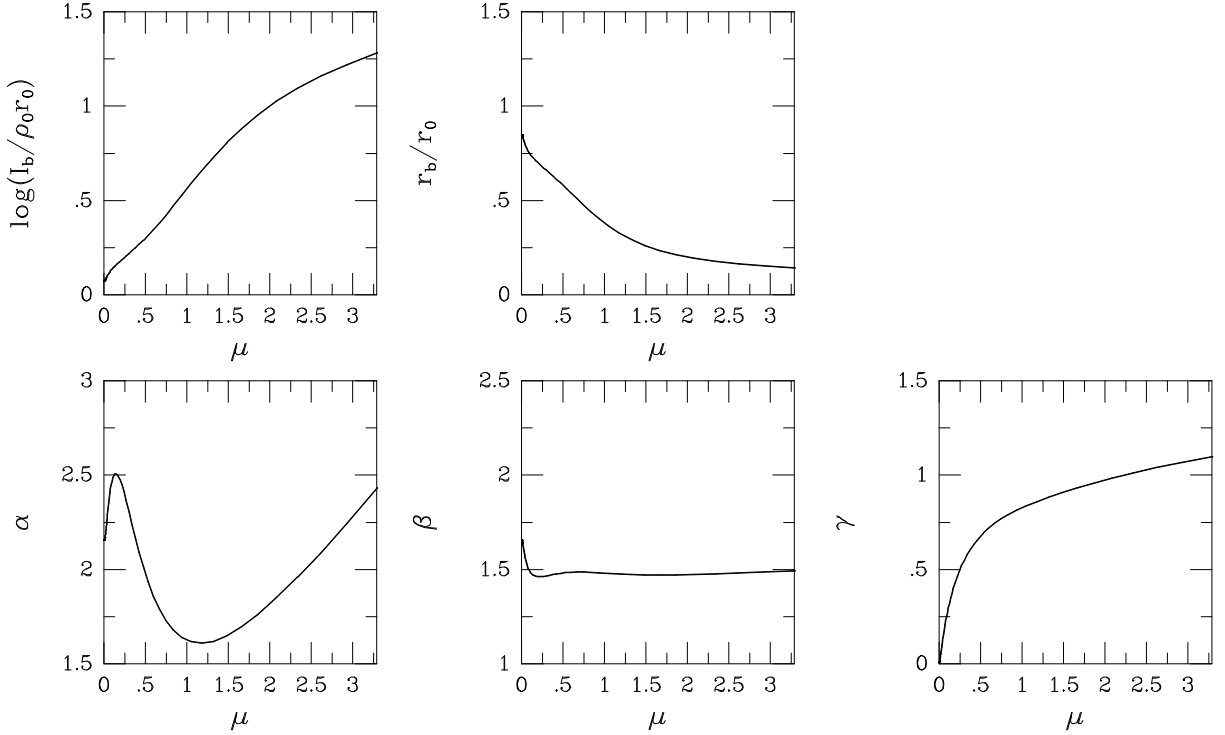


Fig. 2.— Parameters of nuker-law fits to the predicted intensity profiles for models of adiabatic BH growth in an isothermal sphere, as function of the dimensionless BH mass μ . Each fit was performed over the radial range indicated in Figure 1. The quantities r_0 and ρ_0 are the core radius and central density of the initial model.

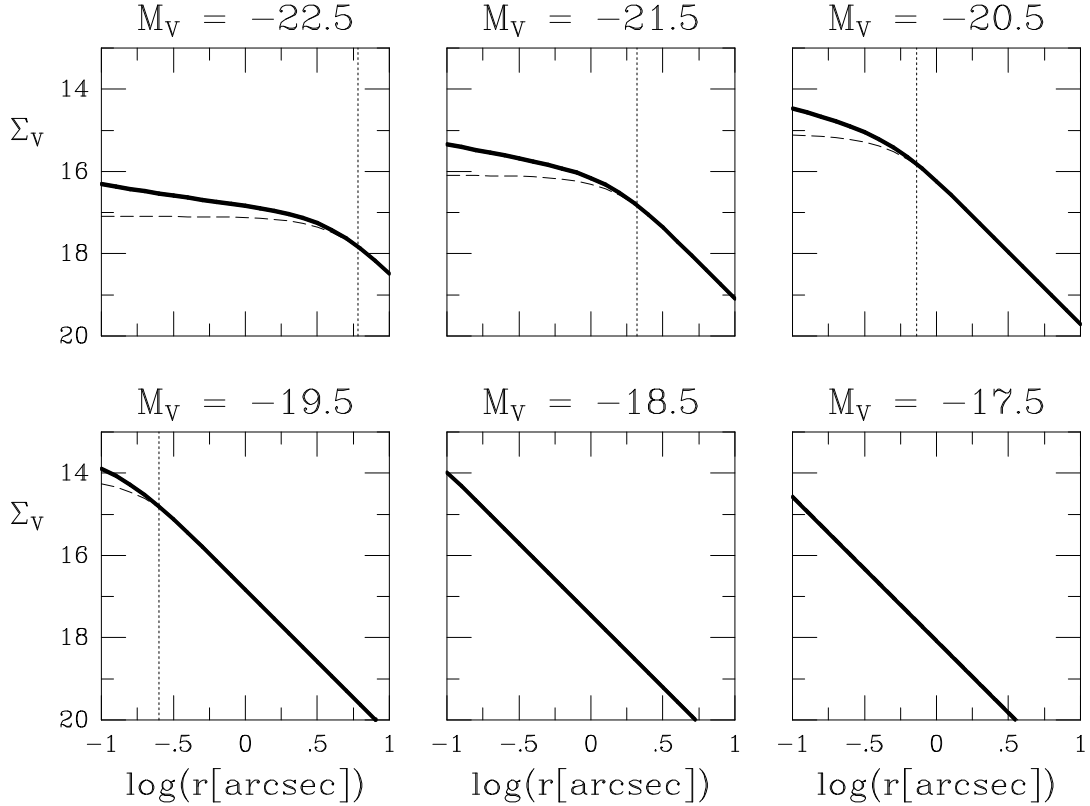


Fig. 4.— Predicted V -band surface brightness profiles $\Sigma_V(r)$ for galaxies of different absolute magnitude, at the distance of the Virgo cluster. The parameters r_0 and $\rho_0 r_0$ for each model were obtained from the scaling relations given in the text, which are based on observations of large samples of galaxies. Dashed curves show the model profiles before BH growth. Heavy solid curves show the model profiles after adiabatic growth of a BH with mass given by equation (5). Each panel shows the radial range from $0.1''$ to $10''$, which is the range typically accessible with HST. A dotted vertical line in each panel indicates the core radius r_0 of the initial model. This radius is too small to be observable ($r_0 < 0.1''$) for $M_V = -18.5$ and $M_V = -17.5$. The models naturally explain the observed transition from core profiles to power-law profiles with decreasing luminosity.

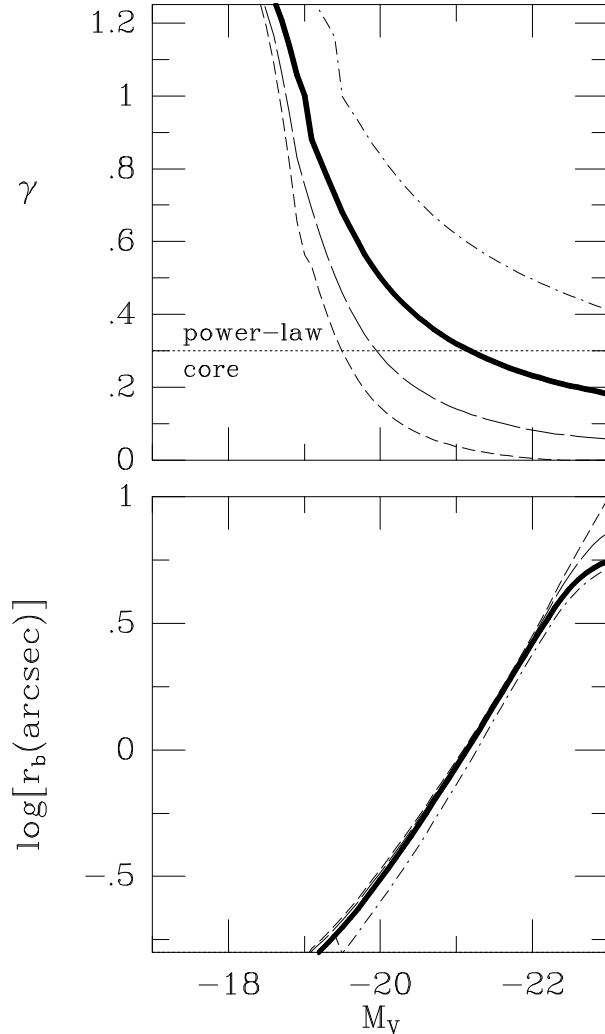


Fig. 5.— Nuker-law parameters for model galaxies of different absolute magnitude, at the distance of the Virgo cluster. The models assume adiabatic BH growth and the scaling relations given in the text. The top panel shows the central cusp slope γ , the bottom panel the break radius r_b . The parameterizations were fit over the radial range between $0.1''$ and $10''$, which is the range typically accessible with HST. Heavy solid curves show the predictions for models with BH masses given by equation (5) (corresponding to the heavy solid profiles in Figure 4). Dashed curves show the predictions for the initial isothermal models, i.e., for models without BHs (corresponding to dashed profiles in Figure 4). The long-dashed curves show the predictions for models that have three times smaller BH masses than indicated by equation (5); the dash-dot curves show the predictions for models that have three times larger BH masses than indicated by this equation. A dotted horizontal line in the top panel indicates the boundary between core galaxies and power-law galaxies. A galaxy is defined to be a core galaxy only if it has both $\gamma \leq 0.3$ and $\log r_b \geq -0.8$ ($r_b \geq 0.16''$); it is a power-law galaxy otherwise (F97).

(Figure on next two pages)

Fig. 6.— V -band surface brightness profiles for the core galaxies in the sample. The heavy solid curve for each galaxy is the nuker law that best fits the HST photometry. Dashed curves are the best-fitting adiabatic BH growth models. Dotted curves show the isothermal brightness profiles of the models *before* BH growth. Dashed curves are generally invisible at small radii, because they overly the solid curves (indicating a good fit). Dotted curves are generally invisible at large radii, because they overly the dashed curves (indicating that the BH has no effect at large radii). To obtain the dashed profiles from the dotted profiles through adiabatic BH growth requires the BH masses listed in Table 1. The brightness profiles in the hatched regions are uninfluenced by the BH growth, and were excluded from the fit. In these regions the models often represent the data poorly because an isothermal sphere is known to be a poor approximation to the large radii behavior of real galaxies. The fits at large radii can be improved by studying models with more general initial conditions, but this is expected to have little effect on the inferred BH masses.

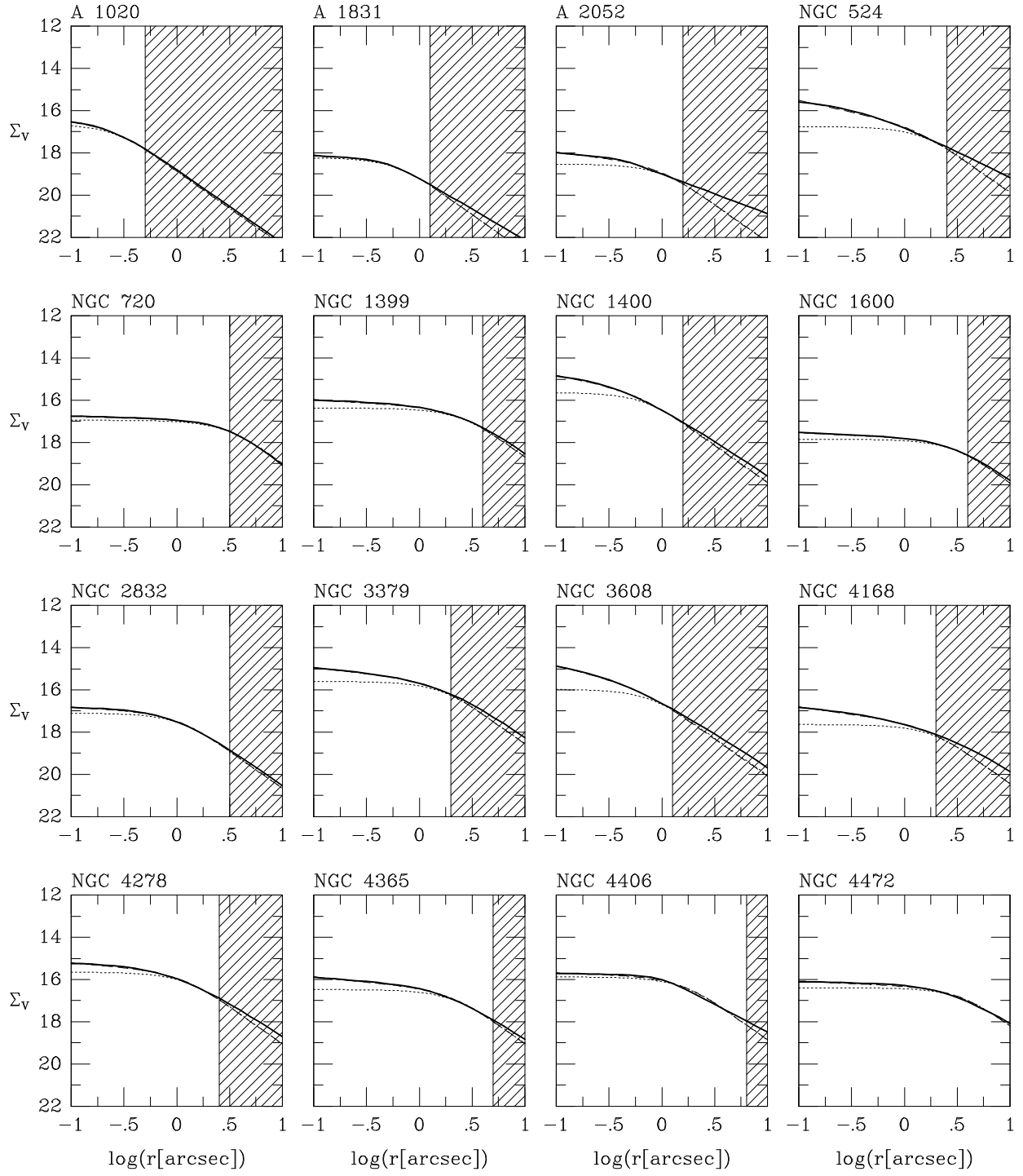


Fig. 6.— (first part).

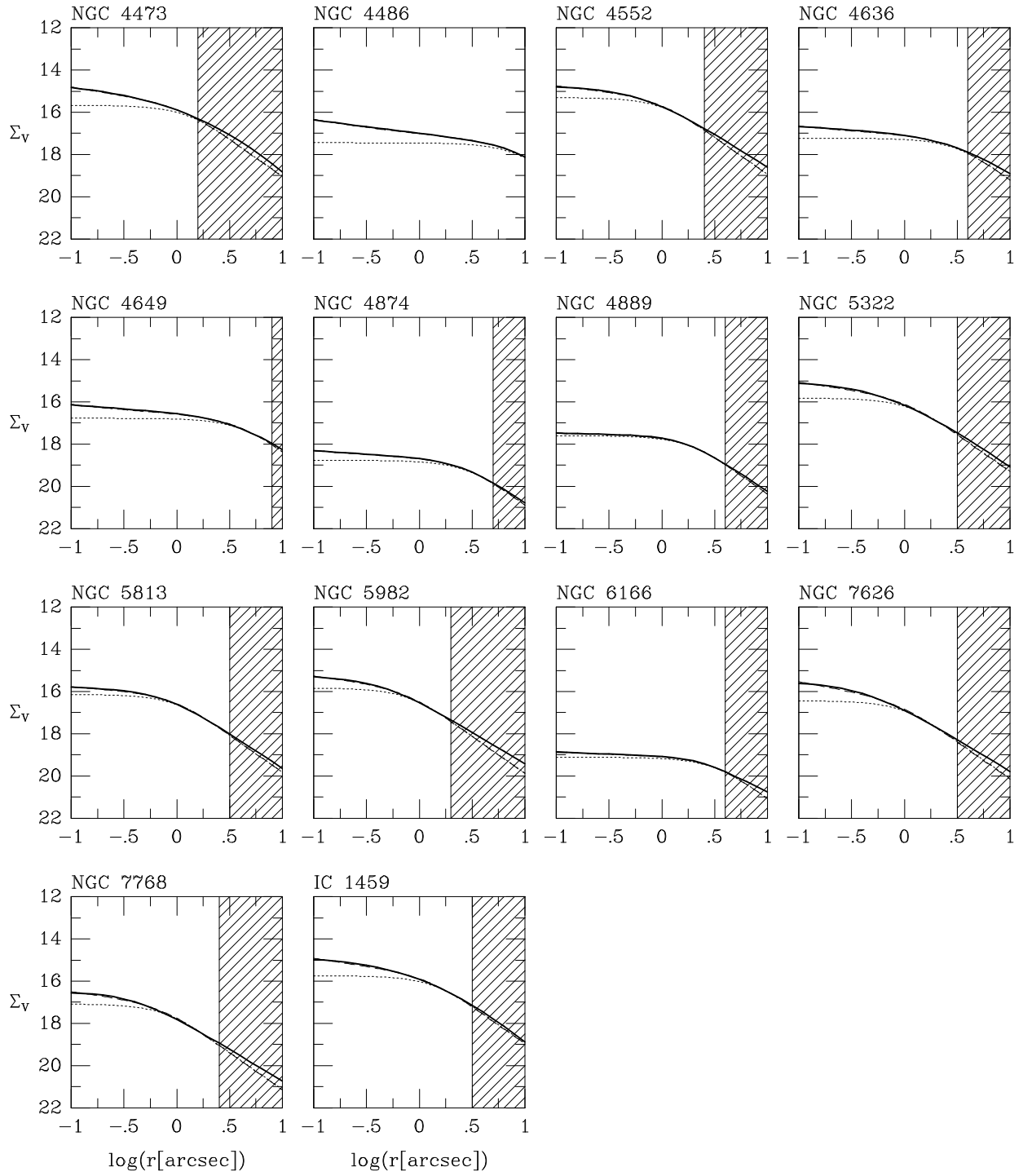


Fig. 6.— (second part).

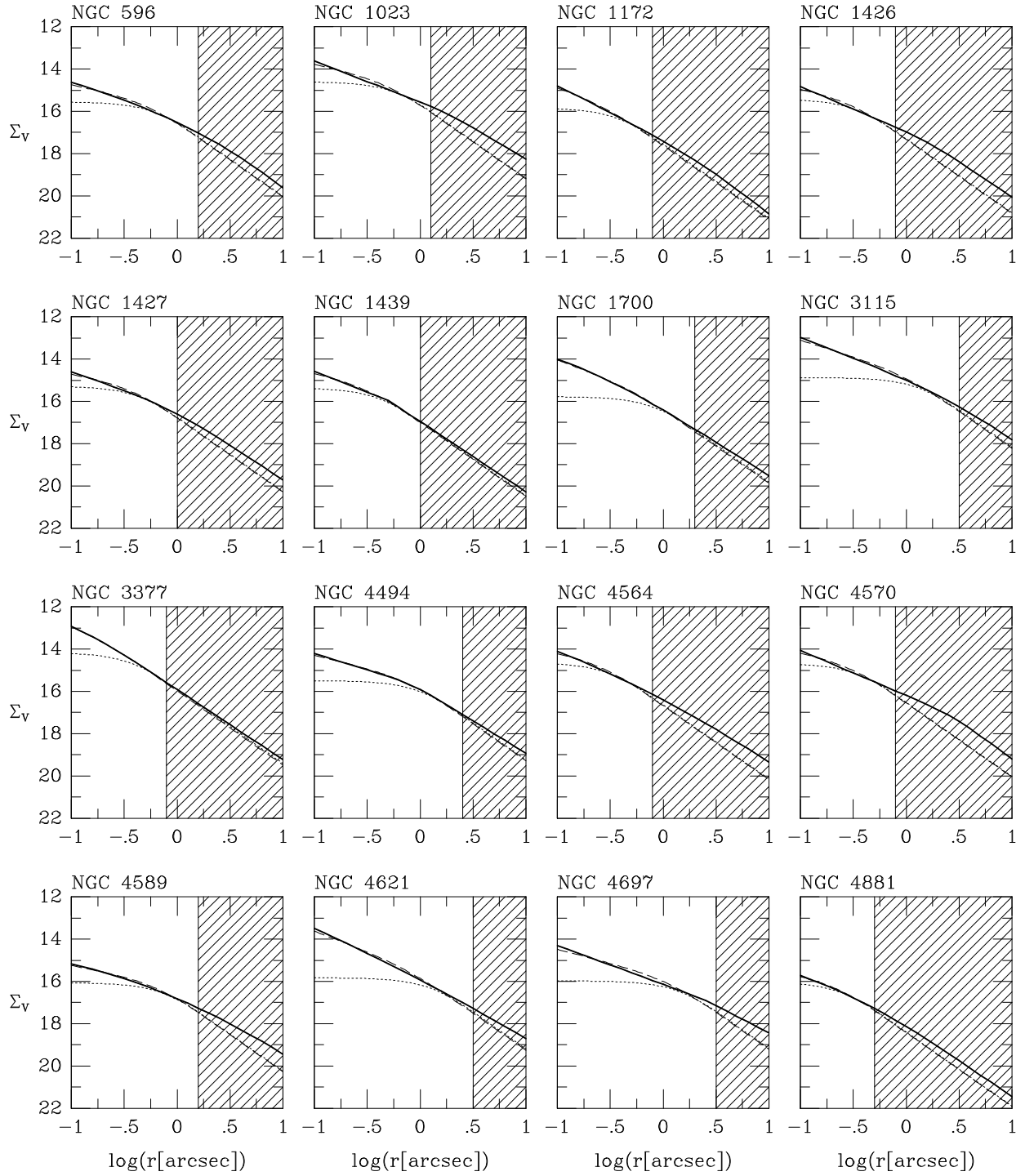


Fig. 7.— As Figure 6, but now for the power-law galaxies in the sample.

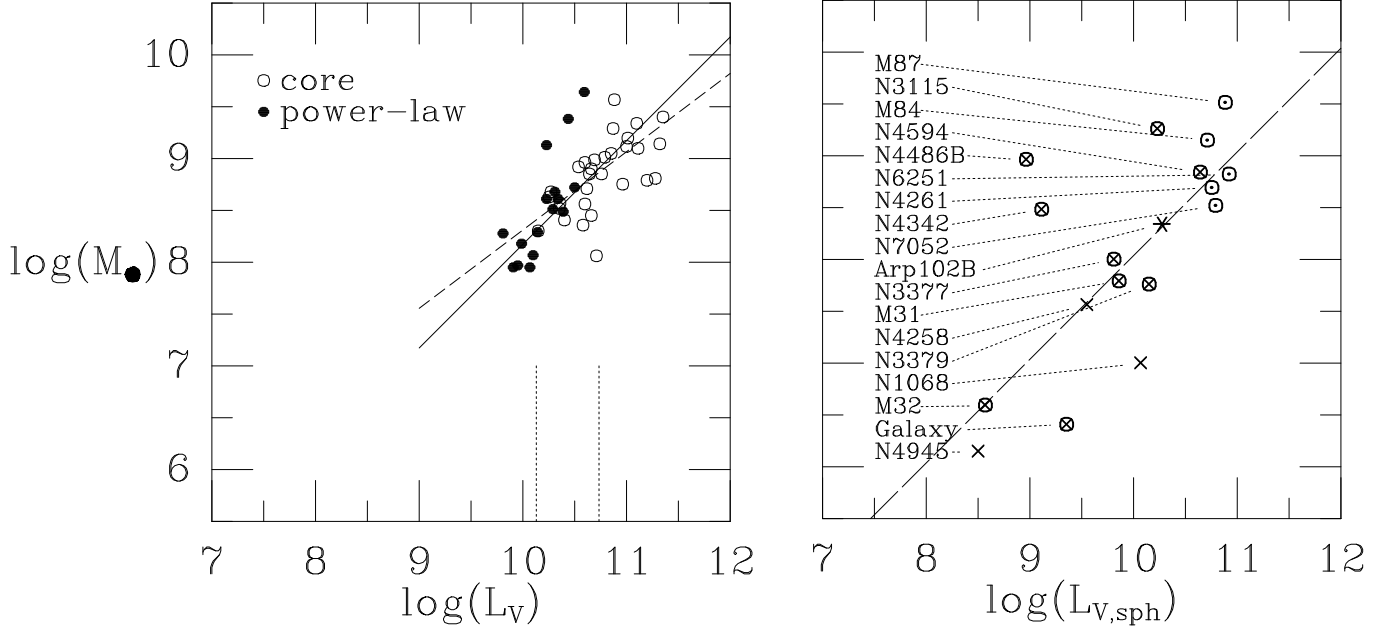


Fig. 8.— (a) BH mass distribution as function of V -band galaxy luminosity for the sample of early-type galaxies in Tables 1 and 2, inferred from adiabatic BH growth models for HST photometry. Core galaxies and power-law galaxies are indicated by open and closed symbols, respectively. The dashed line is the best least-squares fit to the data. The solid line is the best fit line of unit slope. Vertical dotted lines indicate the luminosities corresponding to $M_V = -20.5$ and $M_V = -22$. (b) BH mass distribution as function of V -band *spheroid* luminosity for nearby galaxies with kinematically detected BHs (adapted from figure 1a of van der Marel 1998, which also lists the references for the individual galaxies). These M_{\bullet} values are typically believed to be accurate to $|\Delta \log M_{\bullet}| \lesssim 0.3$. The symbol type indicates the kinematical tracer used to measure the BH mass: (\odot) ionized gas kinematics of nuclear disks; (\otimes) stellar kinematical studies; (\times) radio observations of water masers; ($*$) time variability of broad double-peaked Balmer lines. The long-dashed line is the best fit line of unit slope; it is consistent with the solid line in the left panel to within 0.13 dex.

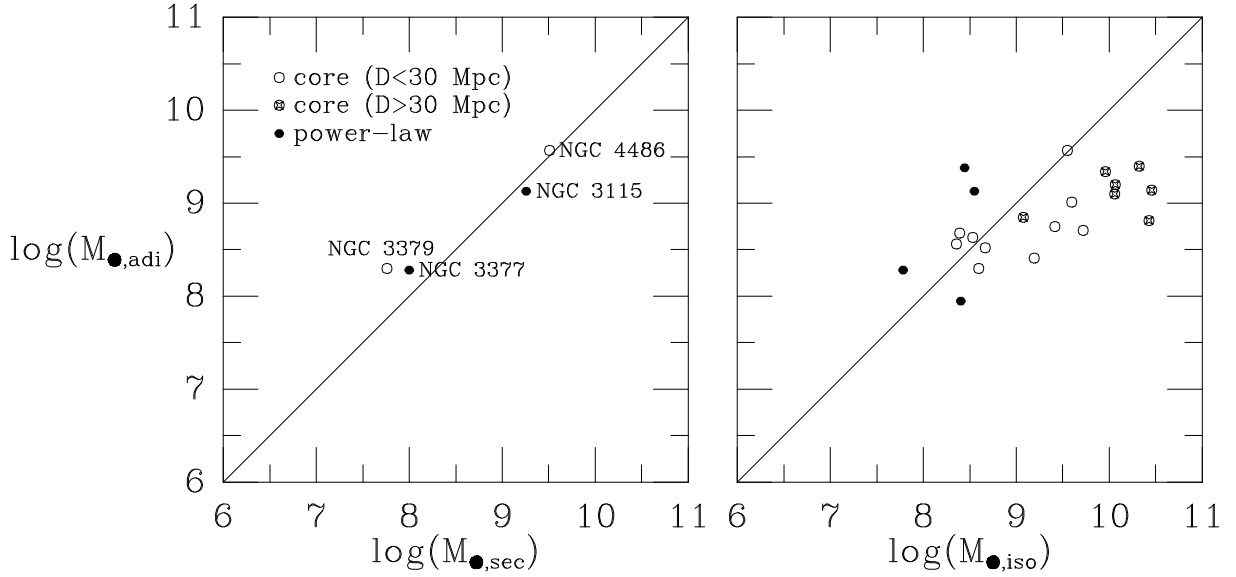


Fig. 9.— Comparison of BH masses $M_{\bullet,\text{adi}}$ inferred from the adiabatic BH growth models (shown along the ordinate) to kinematically determined BH masses. The left panel shows galaxies with kinematically determined BH masses $M_{\bullet,\text{sec}}$ that are ‘securely’ known from HST spectroscopy. The right panel shows galaxies for which BH masses $M_{\bullet,\text{iso}}$ were estimated from isotropic stellar dynamical models for ground-based stellar kinematics (M98). All BH masses are in M_{\odot} . The accuracy of the $M_{\bullet,\text{sec}}$ values is believed to be better than 0.3 dex. The formal errors in $M_{\bullet,\text{adi}}$ and $M_{\bullet,\text{iso}}$ are small (typically $\lesssim 0.10$ dex), but the accuracy of these estimates is determined entirely by the unknown accuracy of the underlying model assumptions. Different symbols indicate core galaxies closer than 30Mpc, core galaxies further than 30Mpc, and power-law galaxies, respectively. The solid lines indicate where the BH masses from different methods would agree perfectly.

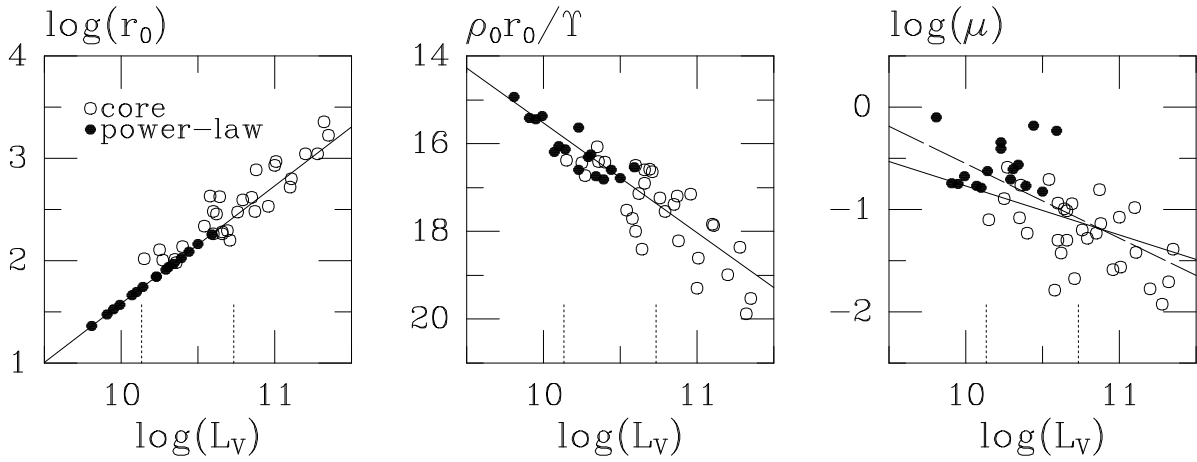


Fig. 10.— Adiabatic BH growth model parameters for the sample galaxies as function of V -band galaxy luminosity. Shown from left to right are the progenitor core radius r_0 in pc, the progenitor core intensity scale $\rho_0 r_0 / \Upsilon$ in $\text{mag}/\text{arcsec}^2$, and the dimensionless BH mass μ . The solid lines are the predicted scaling relations from equations (4) and (7). The core radius r_0 for power-law galaxies was not obtained from a fit to the data, but was fixed a priori to lie on the solid line, as described in the text. The long-dashed line in the right panel shows the scaling relation obtained by combining equations (4) and (6) with equation (9). In the scenario discussed here, the homogeneous progenitor cores of core galaxies and power-law galaxies follow a single set of nuclear scaling relations.

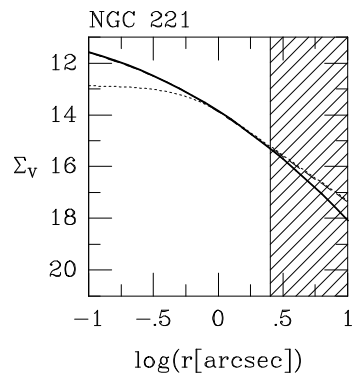


Fig. 11.— Observed and model surface brightness profiles for M32, with line types as in Figure 6.

Table 1. Sample properties and model results for core galaxies

name	source	D (Mpc)	M_V	$\log L$ (L_\odot)	r_0 ($''$)	$\rho_0 r_0 / \Upsilon$ (mag/ $['']^2$)	$\log \mu$	$\log(M_\bullet / \Upsilon)$ (L_\odot)	$\log M_\bullet$ (M_\odot)	RMS (mag/ $['']^2$)
(1)	(2)	(3)	(4)	(5)	(6)	(7)	(8)	(9)	(10)	(11)
A 1020	F97	243.8	-22.29	10.85	0.35	17.39	-1.23	8.22	9.05	0.00
A 1831	F97	280.9	-23.16	11.20	0.81	18.99	-1.77	7.90	8.79	0.01
A 2052	F97	132.0	-22.66	11.00	1.34	19.29	-1.08	8.26	9.12	0.04
NGC 524	F97	23.1	-21.51	10.54	1.95	17.52	-0.71	8.15	8.92	0.05
NGC 720	F97	22.6	-21.62	10.58	3.91	17.71	-1.78	7.58	8.36	0.00
NGC 1399	F97	17.9	-21.71	10.62	3.29	17.13	-1.42	7.82	8.71	0.02
NGC 1400	F97	21.5	-21.06	10.36	0.92	16.40	-0.76	7.83	8.57	0.03
NGC 1600	F97	50.2	-22.70	11.01	3.85	18.61	-1.56	8.12	9.20	0.01
NGC 2832	F97	90.2	-22.95	11.11	1.45	17.87	-1.42	8.22	9.10	0.03
NGC 3379	F97	9.9	-20.55	10.15	2.17	16.37	-1.10	7.57	8.30	0.01
NGC 3608	F97	20.3	-20.84	10.27	1.03	16.73	-0.59	7.91	8.68	0.02
NGC 4168	F97	36.4	-21.76	10.64	2.40	18.40	-0.99	8.08	8.85	0.02
NGC 4278	C97	17.5	-21.16	10.40	1.62	16.42	-1.23	7.66	8.41	0.03
NGC 4365	F97	22.0	-22.06	10.76	2.80	17.24	-1.20	8.04	8.85	0.03
NGC 4406	C97	15.3	-21.94	10.71	2.13	16.64	-1.67	7.25	8.06	0.07
NGC 4472	F97	15.3	-22.57	10.96	4.57	17.15	-1.59	7.80	8.75	0.05
NGC 4473	B96	15.8	-20.80	10.25	1.66	16.43	-0.89	7.92	8.63	0.02
NGC 4486	F97	15.3	-22.38	10.88	10.35	18.21	-1.14	8.53	9.57	0.02
NGC 4552	F97	15.3	-21.05	10.35	1.38	16.07	-1.08	7.69	8.52	0.04
NGC 4636	F97	15.3	-21.67	10.60	4.09	17.99	-1.30	7.65	8.56	0.02
NGC 4649	F97	15.3	-22.14	10.79	5.32	17.54	-1.28	8.08	9.01	0.02
NGC 4874	F97	93.3	-23.54	11.35	3.73	19.53	-1.39	8.44	9.40	0.01
NGC 4889	F97	93.3	-23.36	11.28	2.45	18.36	-1.93	8.00	8.81	0.01
NGC 5322	C97	26.3	-21.90	10.69	1.54	16.58	-0.94	8.19	8.99	0.04
NGC 5813	F97	28.3	-21.81	10.66	1.33	16.90	-1.30	7.65	8.45	0.03
NGC 5982	C97	37.4	-21.83	10.66	1.06	16.59	-1.01	8.10	8.90	0.03
NGC 6166	F97	112.5	-23.47	11.32	4.15	19.88	-1.71	8.24	9.14	0.01
NGC 7626	C97	46.4	-22.34	10.87	1.34	17.20	-0.81	8.45	9.29	0.05
NGC 7768	F97	103.1	-22.93	11.10	1.05	17.84	-0.98	8.50	9.34	0.05
IC 1459	C97	20.7	-21.68	10.60	1.83	16.50	-0.94	8.17	8.96	0.04

Note. — Column (1) is the galaxy name. ‘A’ objects are first-brightest Abell cluster galaxies. Column (2) indicates the source of the nuker-law parameters used in this paper; Faber et al. (1997) [F97], Carollo et al. (1997) [C97] or Byun et al. (1996) [B96]. Columns (3)–(5) list the distance, absolute V -band magnitude and total V -band luminosity, respectively, generally taken from the source in column (2). Columns (6)–(8) list the parameters of the best-fitting adiabatic BH growth model: the core radius r_0 and intensity scale $\rho_0 r_0 / \Upsilon$ of the initial isothermal model, both in observed units, and the dimensionless BH mass μ . Columns (9) and (10) list the implied M_\bullet / Υ and M_\bullet in physical units. The V -band mass-to-light ratio Υ was taken from Magorrian et al. (1998), where available, and otherwise from equation (6). Column (11) lists the RMS residual of the adiabatic BH growth model fit to the observed nuker-law parameterization, over the non-hatched region in Figure 6 or 7. All quantities assume $H_0 = 80 \text{ km s}^{-1} \text{ Mpc}^{-1}$.

Table 2. Sample properties and model results for power-law galaxies

name	source	D (Mpc)	M_V	$\log L$ (L_\odot)	r_0 ($''$)	$\rho_0 r_0 / \Upsilon$ (mag/ $['']^2$)	$\log \mu$	$\log(M_\bullet / \Upsilon)$ (L_\odot)	$\log M_\bullet$ (M_\odot)	RMS (mag/ $['']^2$)
(1)	(2)	(3)	(4)	(5)	(6)	(7)	(8)	(9)	(10)	(11)
NGC 596	F97	21.2	-20.90	10.29	0.80	16.31	-0.71	7.78	8.51	0.10
NGC 1023	F97	10.2	-20.14	9.99	0.75	15.37	-0.67	7.50	8.18	0.13
NGC 1172	F97	29.8	-20.74	10.23	0.48	16.60	-0.34	7.89	8.61	0.07
NGC 1426	F97	21.5	-20.35	10.07	0.44	16.19	-0.77	7.26	7.95	0.11
NGC 1427	C97	17.9	-20.43	10.10	0.57	16.05	-0.79	7.37	8.07	0.09
NGC 1439	C97	21.5	-20.51	10.14	0.53	16.13	-0.63	7.59	8.29	0.05
NGC 1700	F97	35.5	-21.65	10.59	1.05	16.54	-0.23	8.85	9.64	0.04
NGC 3115	F97	8.4	-20.75	10.23	1.72	15.64	-0.40	8.21	9.13	0.10
NGC 3377	F97	9.9	-19.70	9.81	0.48	14.93	-0.10	7.83	8.28	0.02
NGC 4494	C97	14.0	-20.94	10.31	1.27	16.25	-0.61	7.95	8.68	0.04
NGC 4564	F97	15.3	-19.94	9.91	0.40	15.41	-0.75	7.23	7.95	0.09
NGC 4570	F97	15.3	-20.04	9.95	0.45	15.45	-0.75	7.30	7.97	0.11
NGC 4589	C97	22.9	-21.14	10.39	0.96	16.82	-0.77	7.74	8.49	0.09
NGC 4621	F97	15.3	-21.27	10.44	1.64	16.59	-0.18	8.54	9.38	0.10
NGC 4697	F97	10.5	-21.03	10.34	1.84	16.74	-0.56	7.87	8.61	0.15
NGC 4881	B96	93.3	-21.41	10.50	0.32	16.79	-0.83	7.95	8.72	0.06

Note. — See notes to Table 1 for descriptions of the table entries. The progenitor core radius r_0 for power-law galaxies was not obtained from a fit to the data, but was fixed a priori to the value predicted by equation (4), as motivated in the text.

Table 3. Properties and model results for M32

name	source	D (Mpc)	M_V	$\log L$ (L_\odot)	r_0 ($''$)	$\rho_0 r_0 / \Upsilon$ (mag/ $['']^2$)	$\log \mu$	$\log(M_\bullet / \Upsilon)$ (L_\odot)	$\log M_\bullet$ (M_\odot)	RMS (mag/ $['']^2$)
(1)	(2)	(3)	(4)	(5)	(6)	(7)	(8)	(9)	(10)	(11)
NGC 221	-	0.8	-16.60	8.57	0.81	13.63	-0.38	6.34	6.68	0.02

Note. — See notes to Table 1 for descriptions of the table entries. The dash in column (2) indicates that the nuker-law parameters for M32 were not taken from a published source, but were obtained from a new nuker-law fit to the data of Lauer et al. (1992b). The parameters of this fit are: $r_b = 1.58''$, $I_b = 14.77$ mag/arcsec², $\alpha = 0.50$, $\beta = 2.89$ and $\gamma = 0.00$. The progenitor core radius r_0 of the adiabatic BH growth model in column (6) was not fixed a priori (by contrast to the approach adopted for other power-law galaxies) but was obtained from a fit to the data.